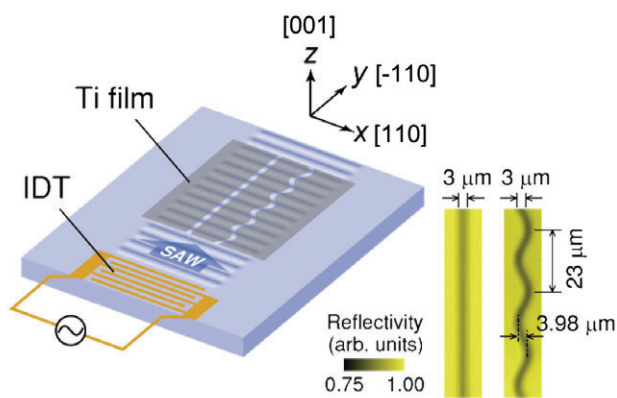


Research Activities in NTT Basic Research Laboratories

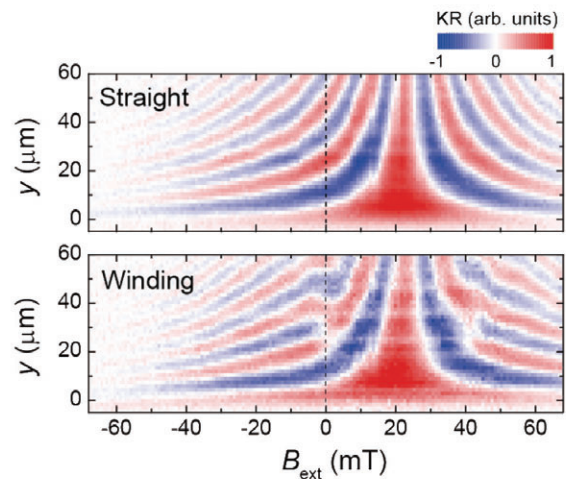
Volume 23
Fiscal 2012

July 2013

NTT Basic Research Laboratories,
Nippon Telegraph and Telephone Corporation (NTT)
<http://www.brl.ntt.co.jp/>



Schematic view of the sample (left) and optical reflectivity images of the straight and winding channels (right).

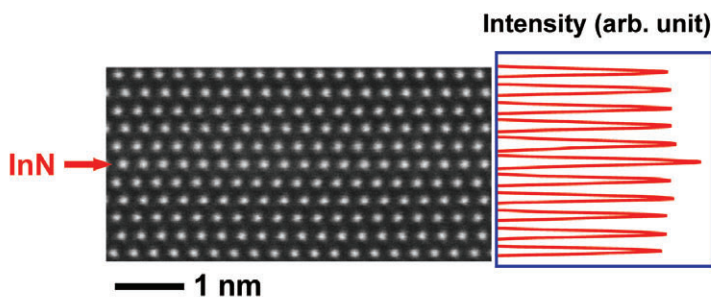


Kerr rotation signals for the straight (upper) and winding (lower) channels plotted as a function of external magnetic field and transport distance.

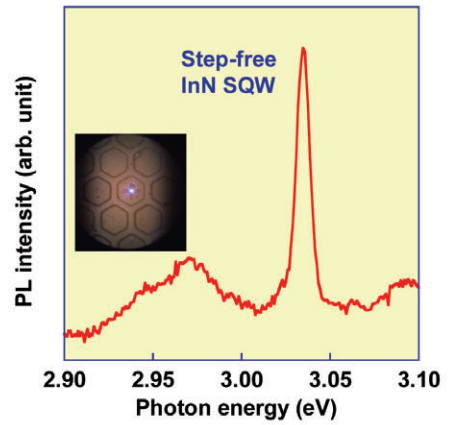
Cover photograph:

Coherent Manipulation of Moving Electron Spins Using Magnetic-Field-Free Electron Spin Resonance

An electron moving in semiconductors experiences a spin-orbit effective magnetic field that depends on the moving direction. We performed Kerr microscopy to measure the spin dynamics of the electrons travelling along a winding semiconductor channel. The experimental results revealed that the resultant spin dynamics is equivalent to the usual electron spin resonance but requires neither static nor time-dependent real magnetic fields. (Page 41)



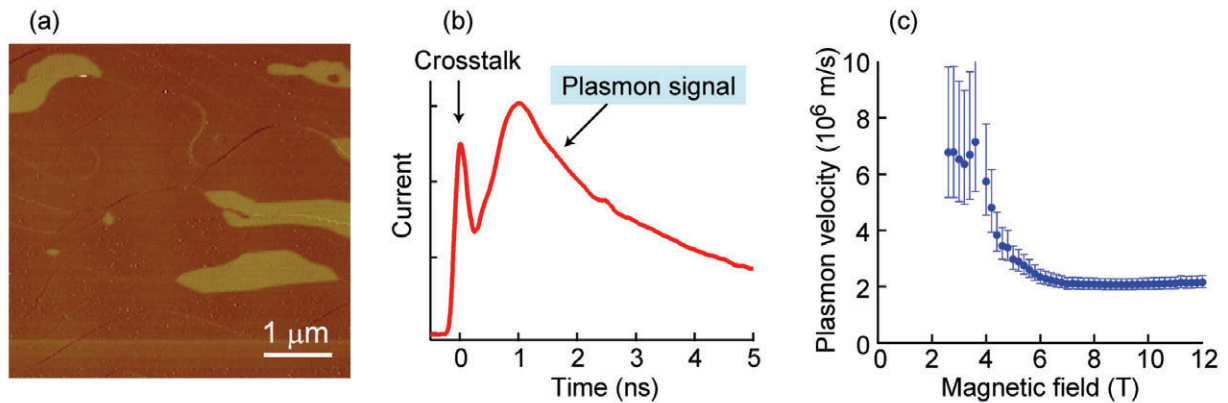
Lattice image and scattering intensity of ultrathin *step-free* InN SQW.



Micro-PL spectrum of ultrathin *step-free* InN SQW.

Extremely Narrow Violet Photoluminescence Line from Ultrathin InN Single Quantum Well on *Step-free* GaN Surface

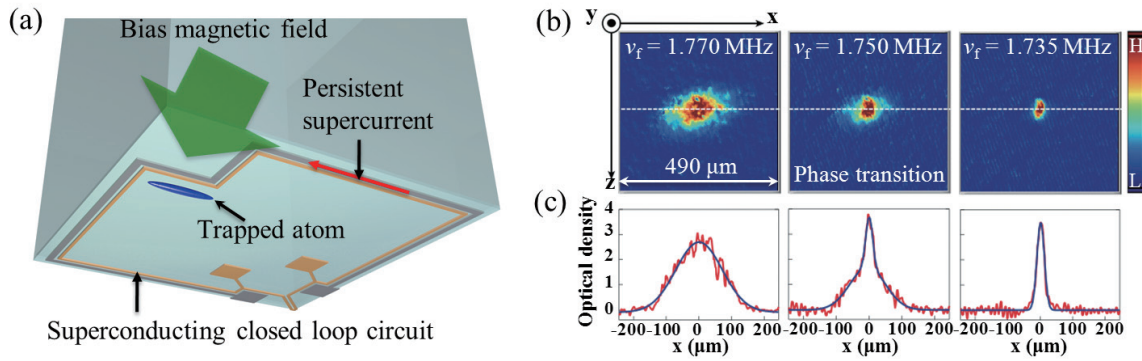
We have successfully fabricated an ultrathin *step-free* InN single quantum well (SQW) that emits highly monochromatic ultraviolet light. The *step-free* InN SQW has one-monolayer (1ML)-thick InN sandwiched by GaN barrier layers and has abrupt hetero-interfaces without any monolayer steps. The abrupt hetero-interfaces enable us to control precisely the emission wavelength and line width by utilizing the quantum size effect. 2ML- and 3ML-thick *step-free* InN SQWs will emit sharp green and red lights as predicted by theoretical calculations. (Page 18)



(a) AFM phase image of graphene grown on SiC. (b) Time evolution of the plasmon signal. (c) Plasmon velocity as a function of the magnetic field.

Plasmon Transport in Graphene Investigated by Time-Resolved Electrical Measurements

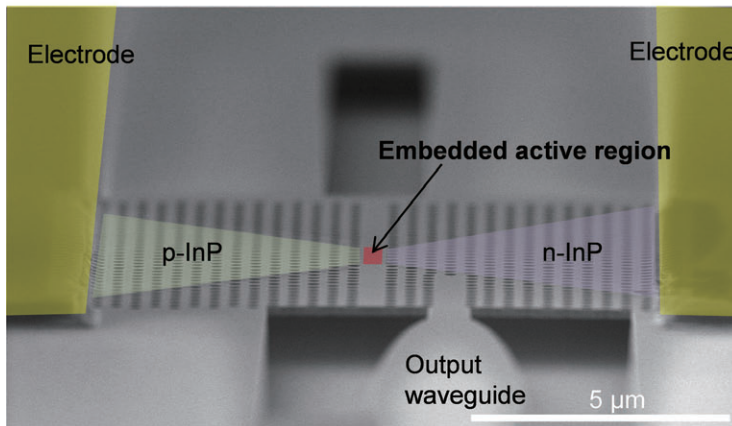
We showed that the velocity of plasmons in graphene can be controlled over two orders of magnitude by applying the magnetic field, screening the plasmon electric field with a gate metal, and changing the carrier density. The wide tunability of the plasmon velocity encourages designing graphene nanostructures for plasmonic circuits. (Page 33)



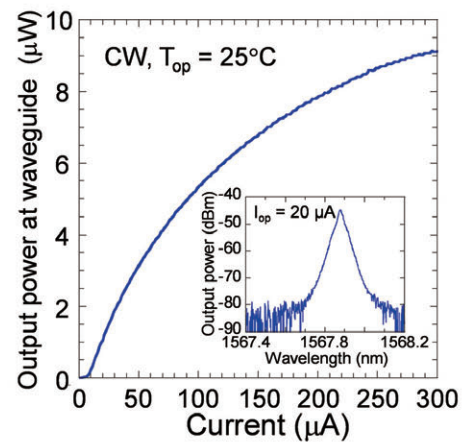
(a) Schematic diagram of atoms trapped on a persistent-supercurrent atom chip.
 (b) TOF images after evaporative cooling. ν_f represents the final radio frequency of the evaporative cooling.
 (c) Cross-sections of the optical density along the dotted line in Fig. (b).

Bose-Einstein Condensate on a Persistent-Supercurrent Atom Chip

We achieved ^{87}Rb Bose-Einstein condensate (BEC) on a persistent supercurrent atom chip by a radio frequency induced evaporative cooling. The condensation was verified by the time-of-flight (TOF) imaging of the bimodal momentum distribution obtained at $\nu_f = 1.750$ MHz. (Page 39)



Scanning electron microscope image



Light-current characteristic and spectrum

Lambda-Scale Embedded Active-Region Photonic-Crystal (LEAP) Lasers

We have developed a photonic-crystal (PhC) nanocavity laser in which a small active region is embedded within an InP-based line defect waveguide. We call this a Lambda-scale Embedded Active-region PhC (LEAP) laser. By using InAlAs for the sacrificial layer in order to reduce the leakage current, we realized a LEAP laser with the lowest threshold current and energy consumption of any semiconductor laser operating at above room temperature. (Page 45)

Message from the Director



We at NTT Basic Research Laboratories (BRL) are extremely grateful for your interest and support with respect to our research activities. BRL's missions are to promote progress in science and innovations in leading-edge technology to advance NTT's business. To achieve these missions, researchers in fields including physics, chemistry, biology, mathematics, electronics, informatics, and medicine, conduct basic research on materials science, physical science and optical science.

Since our management principle is based on an "open door" policy, we are collaborating with many universities and research institutes in Japan, US, Europe, and Asia as well as other NTT laboratories. NTT-BRL organizes international conferences related to quantum physics and nanotechnology and also holds a "Science Plaza" to enhance public understanding of our activities and to ensure a frank exchange of opinions. These activities enable us to realize our missions with respect to the promotion of advances in science and the development of groundbreaking technology for NTT's business. Your continued support will be greatly appreciated.

July, 2013

A handwritten signature in cursive script that reads "Tetsuomi Sogawa". The signature is written in black ink on a white background.

Tetsuomi Sogawa
Director
NTT Basic Research Laboratories

Contents

page

◆ Cover	
◆ Coherent Manipulation of Moving Electron Spins Using Magnetic-Field-Free Electron Spin Resonance	
◆ Color Frontispiece	I
◆ Extremely Narrow Violet Photoluminescence Line from Ultrathin InN Single Quantum Well on <i>Step-free</i> GaN Surface	
◆ Plasmon Transport in Graphene Investigated by Time-Resolved Electrical Measurements	
◆ Bose-Einstein Condensate on a Persistent-Supercurrent Atom Chip	
◆ Lambda-Scale Embedded Active-Region Photonic-Crystal (LEAP) Lasers	
◆ Message from the Director	III
◆ NTT Basic Research Laboratories Organogram	1
◆ Member List	2
I. Research Topics	
◇ Overview of Research in Laboratories	15
◇ Materials Science Laboratory	17
◆ Nitride-Based Semiconductor Light-Emitting Transistors	
◆ Extremely Narrow Violet Photoluminescence Line from Ultrathin InN Single Quantum Well on <i>Step-Free</i> GaN Surface	
◆ Doping Control of AlInN/GaN Lattice-Matched Heterostructure	
◆ Universal Superconducting Ground State in Nd_2CuO_4 and $\text{Nd}_{1.85}\text{Ce}_{0.15}\text{CuO}_4$	
◆ Label-Free Protein Detection on Graphene Oxide Surface	
◆ Epitaxial Trilayer Graphene Mechanical Resonators Obtained by Electrochemical Etching Combined with Hydrogen Intercalation	
◆ Self-Organization of Quasi-Free-Standing Monolayer Graphene Nanoribbon Networks	
◆ Reconstitution of Homomeric GluA2 Receptors in Supported Lipid Membranes: Functional and Structural Properties	
◆ Electrostatic Control of Artificial Cell Membrane Spreading by Tuning the Thickness of an Electric Double Layer in a Nanogap	
◆ Conductive Polymer Combined Wearable Electrodes for Electrocardiography Recordings	
◇ Physical Science Laboratory	27
◆ Donor-Based Single Electron Pump	
◆ Signal Detection Via a Transistor with Steep Current Characteristics	

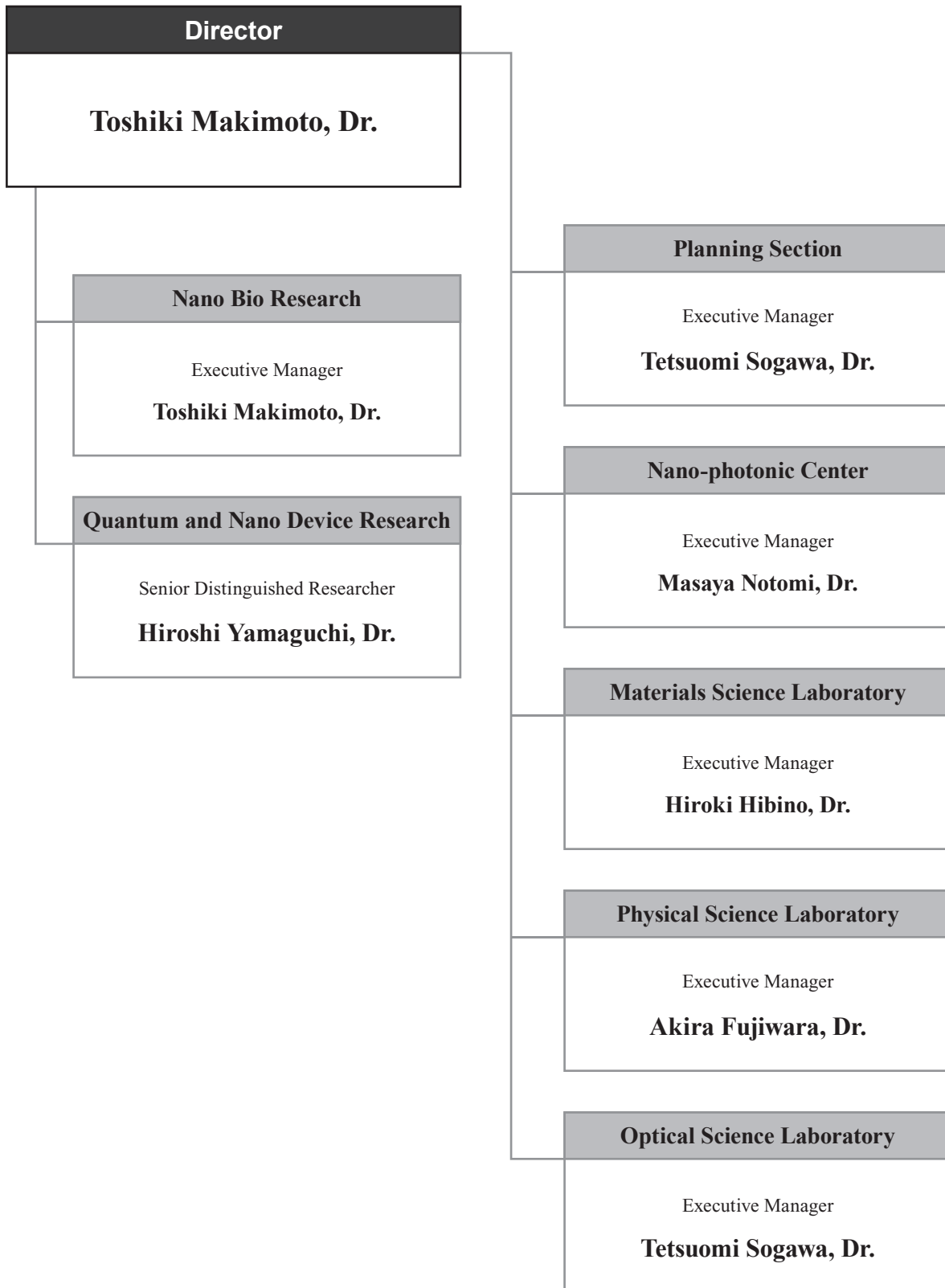
◆ Cavity-Electromechanics with Phonons	
◆ Ferromagnetic-Induced Component in Piezoresistance of GaMnAs	
◆ An Electromechanical Membrane Resonator	
◆ Shot Noise Spectroscopy on a Semiconductor Quantum Dot in the Elastic and Inelastic Cotunneling Regimes	
◆ Plasmon Transport in Graphene Investigated by Time-Resolved Electrical Measurements	
◆ Impact of Graphene Quantum Capacitance on Transport Spectroscopy	
◆ Energy Relaxation Process of a Quantum Memory Coupled with a Superconducting Qubit	
◆ Evidence of a Crossover from Trions to an Electron-Hole Gas	
◇ Optical Science Laboratory	37
◆ Fundamental Limit to Qubit Control with Coherent Field	
◆ Monolithic Source of Polarization Entanglement Using Silicon Photonics	
◆ Bose-Einstein Condensate on a Persistent-Supercurrent Atom Chip	
◆ Ultrafast Surface Electron Dynamics on GaAs(001) Using Time-Resolved Photoelectron Spectroscopy Based on High-Order Harmonic Source	
◆ Coherent Manipulation of Moving Electron Spins Using Magnetic-Field-Free Electron Spin Resonance	
◆ High-Efficiency Detection of Carrier-Envelope Offset Frequency with a Dual-Pitch PPLN Ridge Waveguide	
◇ Nanophotonics Center	43
◆ Ultrafast Spontaneous Emission from Copper-Doped Silicon Nanocavity	
◆ Purcell-Enhanced Single Photon Emission at Telecom Wavelengths from Quantum-Dot Nanocavities	
◆ Lambda-Scale Embedded Active-Region Photonic-Crystal (LEAP) Lasers	
◆ 22-Gbit/s × 16-ch WDM Receiver Based on a Si-Ge-silica Monolithic Photonic Platform	

II. Data

◇ Science Plaza 2012	47
◇ The 7th Advisory Board (Fiscal 2012)	48
◇ Award Winners' List (Fiscal 2012)	49
◇ In-house Award Winners' List (Fiscal 2012)	51
◇ Numbers of Papers, Presentations and Patents (2012)	53
◇ List of Invited Talks at International Conferences (2012)	55

NTT Basic Research Laboratories Organogram

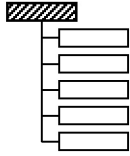
As of March 31, 2013



Member List

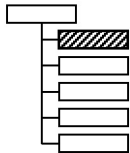
As of March 31, 2013
(* / left NTT BRL during the year)

NTT Basic Research Laboratories



Director, **Dr. Toshiki Makimoto**

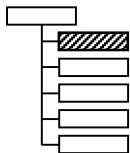
Nano Bio Research



Executive Manager, **Dr. Toshiki Makimoto**

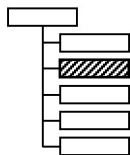
Dr. Keiichi Torimitsu*

Quantum and Nano Device Research



Senior Distinguished Researcher, **Dr. Hiroshi Yamaguchi**

Research Planning Section

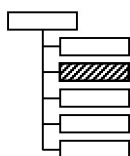


Executive Research Scientist, **Dr. Tetsuomi Sogawa**

Senior Research Scientist, **Dr. Hiroshi Nakashima**
Dr. Hiroki Takesue*

Senior Research Scientist, **Dr. Katsuya Oguri**
Dr. Akihiko Shinya*

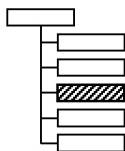
Nano-Photonic Center



Executive Manager, **Dr. Masaya Notomi**

NTT Research Professor, Prof. Yasuhiro Tokura (University of Tsukuba)

Materials Science Laboratory



Executive Manager, **Dr. Hiroki Hibino**

Dr. Tetsuya Akasaka
Dr. Nahoko Kasai*

Thin-Film Materials Research Group:

Dr. Hideki Yamamoto (Group Leader)

Dr. Yasuyuki Kobayashi	Dr. Kazuhide Kumakura	Dr. Hisashi Sato
Dr. Tetsuya Akasaka	Dr. Yoshitaka Taniyasu	Dr. Koji Onomitsu*
Dr. Yoshiharu Krockenberger	Dr. Masanobu Hiroki	
Dr. Kazuyuki Hirama	Dr. Chia-Hung Lin	Dr. Ryan Banal

Low-Dimensional Nanomaterials Research Group:

Dr. Hiroki Hibino (Group Leader)

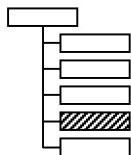
Dr. Fumihiko Maeda	Dr. Kazuaki Furukawa	Dr. Satoru Suzuki
Dr. Hiroo Omi	Dr. Ken-ichi Kanzaki*	Dr. Shin-ichi Tanabe
Dr. Makoto Takamura	Dr. Shengnan Wang	Dr. Yuya Murata
Dr. Carlo M. Orofeo		

Molecular and Bio Science Research Group:

Dr. Koji Sumitomo (Group Leader)

Dr. Akiyoshi Shimada*	Dr. Hiroshi Nakashima*	Dr. Nahoko Kasai
Dr. Yoshiaki Kashimura	Dr. Touichiro Goto	Dr. Aya Tanaka
Dr. Shingo Tsukada		

Physical Science Laboratory



Executive Manager,

Dr. Akira Fujiwara

Dr. Toshiaki Hayashi
Toru Yamaguchi*

Takeshi Karasawa

Nanodevices Research Group:

Dr. Akira Fujiwara (Group Leader)

Dr. Hiroyuki Kageshima

Dr. Gento Yamahata

Dr. Katsuhiko Nishiguchi

Dr. Gabriel Lansbergen*

Dr. Jin-ichiro Noborisaka

Nanostructure Technology Research Group:

Dr. Hiroshi Yamaguchi (Group Leader)

Dr. Kenji Yamazaki

Dr. Koji Onomitsu

Dr. Yuma Okazaki

Toru Yamaguchi

Dr. Hajime Okamoto

Junzo Hayashi

Dr. Imran Mahboob

Daiki Hatanaka

Quantum Solid State Physics Research Group:

Dr. Koji Muraki (Group Leader)

Dr. Kiyoshi Kanisawa

Dr. Toshiaki Hayashi

Dr. Ken-ichi Hitachi*

Dr. Trevor David Rhone

Dr. Satoshi Sasaki

Dr. Takeshi Ohta

Dr. Keiko Takase

Dr. Kyoichi Suzuki

Dr. Norio Kumada

Dr. Takashi Kobayashi

Superconducting Quantum Physics Research Group:

Dr. Hiroshi Yamaguchi (Group Leader)

Dr. Kouichi Semba*

Dr. Shin-ichi Karimoto

Dr. Yuichiro Matsuzaki

Dr. Hayato Nakano

Hirotaka Tanaka

Dr. Xiaobo Zhu*

Dr. Shiro Saito

Dr. Kousuke Kakuyanagi

Spintronics Research Group:

Dr. Akira Fujiwara (Group Leader)

Dr. Tatsushi Akazaki*

Dr. Yuichi Harada

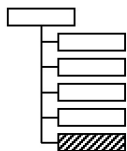
Dr. Yoshiaki Sekine

Dr. Hiroyuki Tamura

Dr. Hiroshi Irie

Dr. Masumi Yamaguchi

Optical Science Laboratory



Executive Manager,

Dr. Tetsuomi Sogawa

Dr. Tetsuya Mukai

Dr. Takehiko Tawara*

Quantum Optical State Control Research Group:

Dr. Kaoru Shimizu (Group Leader)

Dr. Hiroki Takesue

Dr. Hiroyuki Shibata

Dr. Fumiaki Morikoshi

Daisuke Hashimoto

Dr. Hiromitsu Imai

Dr. Toshihiro Kubo*

Dr. Masami Kumagai

Dr. Makoto Yamashita

Dr. Kiyoshi Tamaki

Dr. Nobuyuki Matsuda

Dr. Takahiro Inagaki

Kazuhiro Igeta

Dr. Tetsuya Mukai

Dr. Kensuke Inaba

Dr. Koji Azuma

Dr. William John Munro

Quantum Optical Physics Research Group:

Dr. Tetsuomi Sogawa (Group Leader)

Dr. Hideki Gotoh

Dr. Katsuya Oguri*

Dr. Haruki Sanada

Dr. Yoji Kunihashi

Dr. Kouta Tateno

Dr. Atsushi Ishizawa

Dr. Keiko Kato

Dr. Ken-ichi Sasaki

Dr. Takehiko Tawara

Dr. Guoquiang Zhang

Dr. Ken-ichi Hitachi

Dr. Hiroki Mashiko

Photonic Nano-Structure Research Group:

Dr. Masaya Notomi (Group Leader)

Dr. Atsushi Yokoo

Dr. Hideaki Taniyama

Dr. Masato Takiguchi

Dr. Danang Birowosuto

Dr. Eiichi Kuramochi

Dr. Hisashi Sumikura

Dr. Masaaki Ono

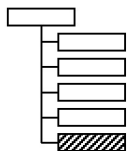
Dr. Xu, Hao

Dr. Akihiko Shinya

Dr. Kengo Nozaki

Dr. Jimyung Kim*

Nano-Photonic Center



Executive Manager, **Dr. Masaya Notomi**

Photonic Nano-Structure Research Team:

Dr. Masaya Notomi	Dr. Akihiko Shinya	Dr. Atsushi Yokoo
Dr. Eiichi Kuramochi	Dr. Hideaki Taniyama	Dr. Hisashi Sumikura
Dr. Kengo Nozaki	Dr. Masato Takiguchi	Dr. Masaaki Ono
Dr. Hiroo Omi	Dr. Takehiko Tawara	Dr. Hiroyuki Shibata
Dr. Nobuyuki Matsuda		

InP Compound Device Research Team:

Dr. Shinji Matsuo	Dr. Takaaki Kakitsuka	Dr. Tomonari Sato
Dr. Koji Takeda	Dr. Koichi Hasebe	

Silicon Photonics Research Team:

Dr. Koji Yamada	Dr. Housei Akazawa	Dr. Tai Tsuchizawa
Hiroshi Fukuda	Rai Kou (Rai Takahashi)	Hidetaka Nishi
Tatsurou Hiraki		

Senior Distinguished Researcher



Masaya Notomi was born in Kumamoto, Japan, on 16 February 1964. He received his B.E., M.E. and Ph.D. degrees in applied physics from University of Tokyo, Japan in 1986, 1988, and 1997, respectively. In 1988, he joined NTT Optoelectronics Laboratories. Since then, his research interest has been to control the optical properties of materials and devices by using artificial nanostructures, and engaged in research on quantum wires/dots and photonic crystal structures. He has been in NTT Basic Research Laboratories since 1999, and currently a group leader of Photonic Nanostructure Research Group and a director of NTT Nanophotonics Center. He is also entitled as Senior Distinguished Scientist of NTT since 2010. In 1996-1997, he was a visiting researcher of Linköping University (Sweden). He was a guest associate professor of Applied Electronics in 2003-2009 and is currently a guest professor of Physics in Tokyo Institute of Technology. He received IEEE/LEOS Distinguished Lecturer Award in 2006, JSPS (Japan Society for the Promotion of Science) prize in 2009, Japan Academy Medal in 2009, The Commendation for Science and Technology by the Minister of Education, Culture, Sports, Science and Technology (Prize for Science and Technology, Research Category) in 2010, and IEEE Fellow grade in 2013. He is serving as a member of National University Corporation Evaluation Committee in the Japanese government. He is also a member of the Japan Society of Applied Physics, APS, IEEE, and OSA.



Hiroshi Yamaguchi was born in Osaka on October 30, 1961. He received the B.E., M.S. in physics and Ph.D. degrees in engineering from the Osaka University in 1984, 1986 and 1993, respectively. He joined NTT Basic Research Laboratories in 1986 and has engaged in the study of compound semiconductor surfaces using electron diffraction and scanning tunneling microscopy. His current interests are micro/nanomechanical devices using semiconductor heterostructures. He was a visiting research fellow in Imperial College, University of London, U.K. during 1995-1996 and a visiting research staff in Paul Drude Institute, Germany in 2003. He is a guest professor in Tohoku University from 2006 and a director of the Japanese Society of Applied Physics in 2008 and 2009. He served as more than 40 committee members of academic societies and international conferences. He received Inoue Prize for Science (2012), Institute of Physics Fellowship (2011), SSDM2009 Paper Award (2010), MNC2008 Outstanding Paper Award (2009), and the Paper Awards of Japan Society of Applied Physics (1989, 2004, 2010). He is currently a group leader of Nanostructure Technology Research Group and Superconducting Quantum Physics Research Group. He is a member of the Japan Society of Applied Physics, the Physical Society of Japan, Institute of Physics (UK), and IEEE.

Distinguished Researchers



Akira Fujiwara was born in Tokyo, Japan on March 9, 1967. He received his B.S., M.S., and Ph.D. degrees in applied physics from The University of Tokyo, Japan in 1989, 1991, and 1994, respectively. In 1994, he joined NTT LSI Laboratories and moved to NTT Basic Research Laboratories in 1996. Since 1994, he has been engaged in research on silicon nanostructures and their application to single-electron devices. He is an executive manager of Physical Science Laboratory and a group leader of Nanodevices Research Group since April 2012. He was a guest researcher at the National Institute of Standards and Technology (NIST), Gaithersburg, MD, USA during 2003-2004. He received the SSDM Young Researcher Award in 1998, SSDM Paper Award in 1999, and Japanese Journal of Applied Physics (JJAP) Paper Awards in 2003 and 2006. He was awarded the Young Scientist Award from the Minister of MEXT (Ministry of Education, Culture, Sports, Science, and Technology) in 2006. He was a director of the Japanese Society of Applied Physics in 2010 and 2011. He is a member of the Japan Society of Applied Physics and the IEEE.



Koji Muraki was born in Tokyo, Japan in 1965. He received his B.S., M.S., and Ph.D. degrees in applied physics from The University of Tokyo, Japan, in 1989, 1991, and 1994, respectively. In 1994, he joined NTT Basic Research Laboratories, Kanagawa, Japan. Since then, he has been engaged in the growth of high-mobility heterostructures and the study of highly correlated electronic states realized in such structures. He was a guest researcher at Max-Planck Institute, Stuttgart, Germany during 2001-2002. He is a member of the Physical Society of Japan and Japan Society of Applied Physics.



Yoshitaka Taniyasu was born in Toyama, Japan on June 10, 1973. He received his B.E., M.E., and Dr. Eng. degrees in electrical engineering from Chiba University, Chiba, Japan in 1996, 1998, and 2001, respectively. He joined NTT Basic Research Laboratories in 2001. He has been engaged in research on epitaxial growth and device application of wide bandgap nitride semiconductors. He was a visiting researcher at Ecole polytechnique fédérale de Lausanne (EPFL) during 2011-2012. He received the Young Scientist Award at the 14th Semiconducting and Insulating Materials Conference (SIMC-XIV) in 2007, and the Young Scientists' Prize from the Minister of Education, Culture, Sports, Science and Technology in 2011, the Young Scientist Award at the 38th International Symposium on Compound Semiconductors (ISCS2011) in 2011, the Best paper Award at the International Workshop on Nitride Semiconductors (IWN2012) in 2012. He is a member of the Japan Society of Applied Physics (JSAP).



Norio Kumada was born in Gifu, Japan in 1975. He received his B.S., M.S., and Ph.D. degrees in physics from Tohoku University, Japan, in 1998, 2000, and 2003, respectively. In 2003, he joined NTT Basic Research Laboratories, Kanagawa, Japan. Since then, he has been engaged in the study of highly correlated electronic states realized in semiconductor heterostructures or in graphene. He received Young Scientist Award of the Physical Society of Japan in 2008 and Young Scientists' Prize from the Minister of Education, Culture, Sports, Science and Technology in 2012. He is a member of the Physical Society of Japan.



Katsuhiko Nishiguchi was born in Hiroshima, Japan in 1975. He received the B.E., M.E., and Ph.D. in electrical engineering in 1998, 2000, and 2002, respectively, from Tokyo Institute of Technology, Tokyo, Japan. Since joining NTT Basic Research Laboratories in 2002, he has been engaged in the research on physics and technology of Si nanometer-scale devices for LSI applications with low power consumption and new functions. He was an invited researcher at the National Center for Scientific Research (CNRS), France during September 2008 and a visiting scientist at Delft University of Technology, the Netherlands during 2012-2013. He received IUPAP Young Author Best Paper Award at the International Conference on Physics of Semiconductors 2000, Graduate Student Award Silver at the Materials Research Society 2000 Fall Meeting, and Young Scientist Award at the Japan Society of Applied Physics Spring Meeting in 2000. He is a member of the Japan Society of Applied Physics.



Shiro Saito was born in Tokyo, Japan in 1972. He received his B.S., M.S., and Dr. Eng. degrees in applied physics from the University of Tokyo, Japan, in 1995, 1997, and 2000, respectively. In 2000, he joined NTT Basic Research Laboratories. Since then, he has been engaged in quantum information processing using superconducting circuits. He was a guest researcher at Delft University of Technology, Delft, the Netherlands during 2005-2006. He has been a guest associate professor in Tokyo University of Science since 2012. He received Young Scientist Award at the Japan Society of Applied Physics Spring Meeting in 2004. He is a member of the Physical Society of Japan and the Japan Society of Applied Physics.

Advisory Board (2012 Fiscal Year)

Name	Affiliation
Prof. Gerhard Abstreiter	Walter Schottky Institute and Physik Department Technische Universität München, Germany
Prof. John Clarke	Physics Department, University of California, Berkeley, U.S.A.
Prof. Evelyn Hu	School of Engineering and Applied Sciences, Harvard University, U.S.A.
Prof. Mats Jonson	Department of Physics, Göteborg University and Heriot-Watt University, Sweden
Prof. Sir Peter Knight	Physics Department, Imperial College/The Kavli Royal Society International Centre Chicheley Hall, U.K.
Prof. Anthony J. Leggett	Department of Physics, University of Illinois, U.S.A.
Prof. Allan H. MacDonald	Department of Physics, The University of Texas, Austin, U.S.A.
Prof. Andreas Offenhäusser	Institute of Complex Systems, Forschungszentrum Jülich, Germany
Prof. Halina Rubinsztein-Dunlop	School of Physical Sciences, University of Queensland, Australia
Prof. Klaus von Klitzing	Max-Planck-Institut für Festkörperforschung, Germany

Invited / Guest Scientists (2012 Fiscal Year)

Name	Affiliation	Period
Dr. Trevor David Rhone	Japan Science and Technology Agency (JST), Japan	Feb. 2012 – Feb. 2013
Prof. Jeremy L O'Brien	University of Bristol, U.K.	Mar. 2012 – May 2012
Prof. Toshihiro Kubo	University of Tsukuba, Japan	Apr. 2012 – May 2012
Prof. Koichi Semba	National Institute of Informatics (NII), Japan	Apr. 2012 – Mar. 2013
Prof. Jorg P. Kotthaus	Ludwig Maximilian University of Munich, Germany	May 2012 – May 2012
Dr. Kenichiro Kusudo	National Institute of Informatics (NII), Japan	May 2012 – Mar. 2013
Dr. Rais Shaikhaidarov	Royal Holloway University of London, U.K.	Oct. 2012 – Nov. 2012
Prof. David Cox	University of Surrey, U.K.	Oct. 2012 – Nov. 2012

Overseas Trainees (2012 Fiscal Year)

Name	Affiliation	Period
Henri Juhani Suominen	The University of Edinburgh, U.K.	Aug. 2011– Jul. 2012
Andy Berry	University of Victoria, Canada	Sep. 2011 – Apr. 2012
Michael Firka	University of Victoria, Canada	Sep. 2011 – Aug. 2012
Elan Michael Grossman	Georgia Institute of Technology, U.S.A.	Jan. 2012 – Aug. 2012
Bennett Eleazer	Georgia Institute of Technology, U.S.A.	Jan. 2012 – Aug. 2012
Yong Fan Jiang	The University of British Columbia, Canada	Jan. 2012 – Aug. 2012
Gediminas Dauderis	Vilnius University, Lithuania	Jan. 2012 – Aug. 2012
Maria Anagosti	University of Gent, Belgium	Jan. 2012 – Aug. 2012
Roger Molto Pallares	Chemical Institute of Sarria (IQS), Spain	Jan. 2012 – Aug. 2012
Sanna Maria Rauhamaki	University of Jyväskylä, Finland	Jan. 2012 – Aug. 2012
Alex Yang	The University of British Columbia, Canada	Jan. 2012 – Aug. 2012
Shibin Thomas	Mahatma Gandhi University, India	Mar. 2012– Mar. 2013
Ahmet Taspinar	Delft University of Technology, Netherlands	Apr. 2012 – Sep. 2012
Robert Amsuss	Vienna University of Technology, Austria	Apr. 2012 – May 2012
David Tregurtha	University of Bath, U.K.	Jun. 2012 – Sep. 2012
Mickael Mounaix	ESPCI ParisTech (École supérieure de physique et de chimie industrielles de la ville de Paris), France	Jul. 2012 – Dec. 2012
Romain Dubourget	ESPCI ParisTech (École supérieure de physique et de chimie industrielles de la ville de Paris), France	Jul. 2012 – Dec. 2012
Ruaridh Forbes	The University of Edinburgh, U.K.	Jul. 2012 – Apr. 2013
Paul Koecher	Oxford University, U.K.	Oct. 2012 – Dec. 2012
Justin Yan	The University of British Columbia, Canada	Jan. 2013 –
Joey Chau	University of Toronto, Canada	Jan. 2013 –
Thomas Ziebarth	University of Victoria, Canada	Jan. 2013 –
Punn Augsornworawat	McGill University, Canada	Jan. 2013 –
Pawel Pactwa	AGH University of Science and Technology, Poland	Jan. 2013 –

Domestic Trainees (2012 Fiscal Year)

Name	Affiliation	Period
Tomohiro Sakai	Keio University	Apr. 2012 – Mar. 2013
Takayuki Watanabe	Tohoku University	Apr. 2012 – Mar. 2013
Shun Dai	University of Tokyo	Apr. 2012 – Mar. 2013
Tatsuya Baba	Tokyo University of Science	Apr. 2012 – Mar. 2013
Rento Osugi	Tohoku University	Apr. 2012 – Mar. 2013
Shun-ichi Matsumoto	Tokyo University of Science	Apr. 2012 – Mar. 2013
Hajime Suzuki	Tokyo University of Science	Apr. 2012 – Mar. 2013
Takanobu Tsunoi	Yokohama National University	Apr. 2012 – Mar. 2013
Takahiko Sato	University of Tokyo	May 2012 – Mar. 2013
Ryonsoku O	The University of Tokushima	Jun. 2012 – Dec. 2012
Keigo Furuta	University of Toyama	Jul. 2012 – Aug. 2012
Wataru Nakayama	Keio University	Jul. 2012 – Aug. 2012
Hiromitsu Chatani	The University of Tokushima	Aug. 2012– Sep. 2012
Takahito Hodumi	Hokkaido University	Aug. 2012– Sep. 2012
Yuji Saito	Tokyo Denki University	Aug. 2012– Mar. 2013
Nuremy Binti Che Ani	Tokyo Denki University	Aug. 2012– Mar. 2013
Miho Yamazaki	Tokyo Denki University	Aug. 2012– Mar. 2013
Huynh Dief Phuoc	Nagaoka University of Technology	Oct. 2012 – Feb. 2013
Shingo Isobe	Nagaoka University of Technology	Oct. 2012 – Feb. 2013
Nobutoshi Yamaguchi	Nagaoka University of Technology	Oct. 2012 – Feb. 2013
Masashi Tachi	Tokyo University of Science	Oct. 2012 – Mar. 2013
Tomoyuki Tahara	Toyohashi University of Technology	Jan. 2013 – Feb. 2013
Shuhei Nakagawa	Toyohashi University of Technology	Jan. 2013 – Feb. 2013
Takahiro Gotoh	Tokyo Denki University	Feb. 2013 – Mar. 2013

I . Research Topics

Overview of Research in Laboratories

Materials Science Laboratory

Hiroki Hibino

This laboratory aims at contributing to progress in materials science and revolutionizing information communication technology by creating new materials and functions through materials design at the atomic and molecular levels.

This laboratory consists of three research groups investigating a wide range of materials such as nitride semiconductors, graphene, superconductors, and biological molecules. We are conducting innovative materials research based on the technologies of growing high-quality thin films and precisely measuring the structure and physical properties of materials.

This year, we succeeded in measuring extremely narrow violet photoluminescence line from ultrathin InN single quantum well on step-free GaN surface, demonstrating label-free protein detection on graphene oxide surface, and achieving electrocardiography simply by wearing a piece of clothing that has textile electrodes combined with conductive polymer.

Physical Science Laboratory

Akira Fujiwara

The aim of this laboratory is to develop semiconductor- and superconductor-based solid-state devices, which will have a revolutionary impact on future communication and information technologies. Utilizing high-quality crystal growth techniques and nanolithography techniques we have developed, five research groups are working on nanodevices, quantum information processing devices, and high-sensitivity sensors based on new degrees of freedom such as single electrons, mechanical oscillations, quantum coherent states, and spins.

This year we succeeded in measuring and controlling the velocity of plasmons in graphene and realizing "cavity-electromechanics" with a nanomechanical resonator, which is a classical analogy of cavity quantum electrodynamics. We also demonstrated the operations of novel devices such as a logic device with an electromechanical membrane resonator and a sensor based on stochastic resonance with silicon nanotransistors.

This laboratory aims for the development of core-technologies that will innovate on optical communications and optical signal processing, and seeks fundamental scientific progresses.

The groups in our laboratory are working for the quantum state control by very weak light, the search for intriguing phenomena using very intensive and short pulse light, and control of optical properties by using photonic crystals and ultrasonic techniques, based on unique properties of semiconductor nanostructures such as quantum dots and nanowires.

In this year, we demonstrated a Bose-Einstein condensate of cold atoms on the superconducting atom chip. We succeeded in generating a polarization entangled photon pair with a high quality by use of an integrated silicon photonic circuit. We also demonstrated that electron spins in semiconductors can be transported and manipulated by using surface acoustic waves and that electron spin resonance can be achieved in the absence of real magnetic fields.

Nanophotonics Center (NPC) was just established in April 2012 by several research groups involved with nanophotonics in NTT Basic Research Laboratories, NTT Photonics Laboratories, and NTT Microsystem Integration Laboratories. We are aiming for developing a full-fledged large-scale photonic integration technology by which we will be able to densely integrate a large number of nano-scale photonic devices with various functions in a single chip. Furthermore, we are targeting extreme reduction of the consumption energy for photonic information processing by taking advantage of the nanophotonics technology.

Currently, we are conducting studies of photonic crystals to reduce the footprint and consumption energy of various photonic devices, such as all-optical switches, all-optical memories, and lasers. We are also studying various photonic nanostructures to ultimately enhance light-matter interactions, and exploiting photonic integrated circuits and devices based on the silicon photonic platform. Furthermore, we are developing ultra-fine nano-fabrication technologies based on electron beam lithography and sophisticated integration technologies of active semiconductors for photonics.

Nitride-Based Semiconductor Light-Emitting Transistors

Kazuhide Kumakura, Hideki Yamamoto, and Toshiki Makimoto
Materials Science Laboratory

Light-emitting transistors (LETs), which are based on high-speed heterojunction bipolar transistors (HBTs) with a quantum well (QW) in the base layer, are electrical devices as well as optical ones [1]. According to the principles of their operation, LETs can run faster than conventional light-emitting diodes (LEDs). Since nitride-based semiconductor LEDs are commercially available for lighting, it is expected that the nitride-based semiconductor LETs will work as light sources for visible light communication [2]. In this work, we fabricated nitride-based semiconductor LETs and investigated their optical output characteristics.

We fabricated pnp AlGaIn/InGaIn/GaN LETs with a 3-nm-thick QW in the base layer. The In mole fraction of the InGaIn QW was higher than that of the InGaIn base layer. When we apply forward bias at the emitter-base junction of the LETs, holes are injected from the emitter to the base layer. The injected holes diffuse toward the collector and are captured at the QW. Some of the uncaptured holes reach the collector. Figure 1 shows a photograph of the emission from the LETs under forward bias conditions. We can observe the strong purplish emission with the peak wavelength of 410 nm. Next, we fabricated three types of LETs with the QW position varied in the base layer: near the emitter, at the center of the base, and near the collector. Figure 2 shows the optical output power as a function of the base current for the three LETs. We also show the output power for a QW-free LET (standard HBT) as a reference. The output power with the QW near the collector is weaker than with it near the emitter. This indicates that the probability of the hole capture depends on the position of the QW. The velocity of the holes diffusing in the base becomes larger as the holes approach the collector, which results in a lower hole capture probability near the collector. We achieved 0.3-mW optical output power from the LET with the QW near the emitter at the base current of 0.3 mA, corresponding to the external quantum efficiency of 3.3 %. We will investigate the electrical and optical modulation properties of the LETs for high-speed operation, which may open an avenue to their application as high-speed visible light sources.

[1] M. Feng et al., *Appl. Phys. Lett.* **84** (2004) 1952.

[2] Y. Tanaka et al., *IEICE Trans. Commun.* **E86-B** (2003) 2440.

[3] K. Kumakura et al., *Int. Conf. Solid State Devices and Materials*, 2011 Nagoya, A-4-2.

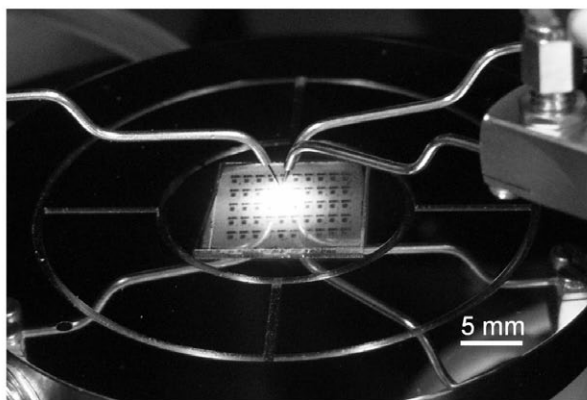


Fig. 1. Photograph of the emission from the LET under forward bias conditions.

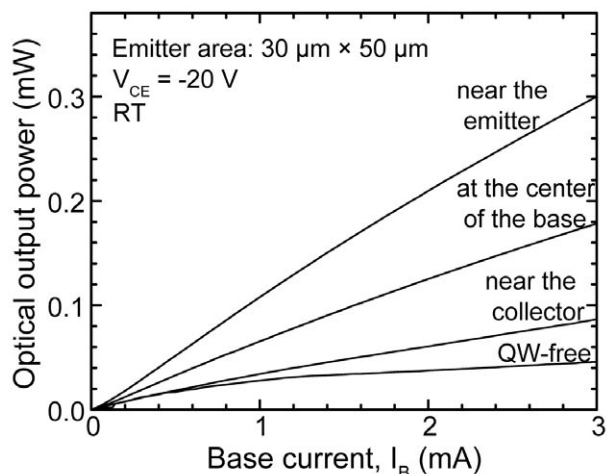


Fig. 2. Optical output power as a function of the base current for the three LETs and a HBT.

Extremely Narrow Violet Photoluminescence Line from Ultrathin InN Single Quantum Well on *Step-Free* GaN Surface

Tetsuya Akasaka, Hideki Gotoh*, Yasuyuki Kobayashi, and Hideki Yamamoto
Materials Science Laboratory, *Optical Science Laboratory

Blue and green light emitting diodes (LEDs) have been achieved with InGaN quantum well (QW) active layers. For a longer wavelength emission, e.g., red emission, InGaN QWs having much higher In composition are required, but the higher In concentration causes severe deterioration of crystalline quality. High-efficiency emission in near-ultraviolet, visible, and near-infrared regions, in principle, can also be achieved by using InN QWs, if the thickness of the ultrathin InN QWs [typically several monolayers (MLs)] can be controlled with an accuracy of a single ML. However, abrupt hetero-interfaces without a single-ML step have not been obtained so far. Recently, we have succeeded in fabricating step-free GaN surfaces 50 μm in diameter without any ML steps by selective-area metalorganic vapor phase epitaxy [1]. In the present study, we investigated the fabrication of step-free InN QWs using step-free GaN surfaces as a template.

Partially coalesced two-dimensional nuclei of InN were formed on a step-free GaN surface by a 10-s InN growth. The coalescence was completed after 30 s and 1-ML-thick step-free InN was eventually formed. Subsequently, a step-free InN single quantum well (SQW) hetero-structure was fabricated by depositing a GaN cap layer onto the step-free InN surface. Figure 1 shows a cross-sectional lattice image of the step-free InN SQW taken by the high-angle annular dark field (HAADF) method in scanning transmission electron microscopy (STEM). In atoms are brighter than Ga atoms, since heavier atoms have stronger scattering intensity. The horizontally integrated scattering intensity of a single line at the center is higher than the others, indicating the formation of 1-ML-thick step-free InN SQW. A micro-photoluminescence spectrum was measured at 4 K for the 1-ML-thick step-free InN SQW (Fig. 2). A sharp single peak is observed with a full width at half maximum of 9 meV at 3.03 eV (violet color) [2]. The peak width is much narrower than that (~ 60 meV) of conventional InGaN QWs emitting a violet light, which is also a hallmark of the abrupt hetero-interfaces and homogenous composition in the step-free InN SQW. 2ML- and 3ML-thick step-free InN SQWs will emit sharp green and red light as predicted by theoretical calculations.

This work was supported by KAKENHI.

[1] T. Akasaka, Y. Kobayashi, and M. Kasu, *Appl. Phys. Express* **3** (2010) 075602.

[2] T. Akasaka, H. Gotoh, Y. Kobayashi, and H. Yamamoto, *Adv. Mater.* **24** (2012) 4296.

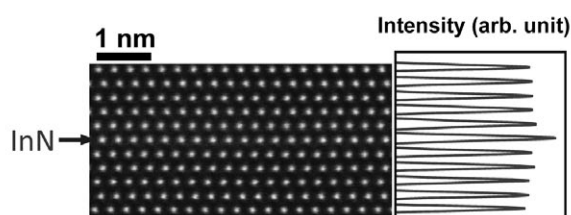


Fig. 1. Lattice image and horizontally integrated scattering intensity of 1-ML-thick step-free InN SQW.

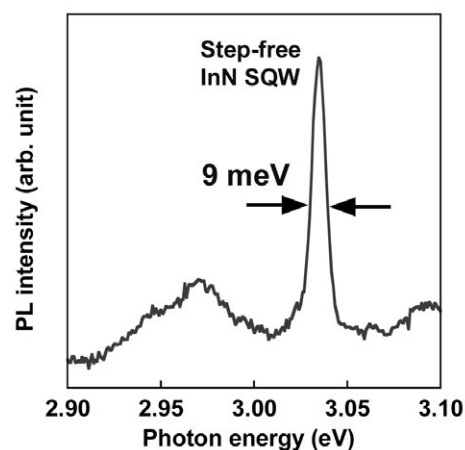


Fig. 2. Micro-photoluminescence spectrum of 1-ML-thick InN SQW measured at 4 K.

Doping Control of AlInN/GaN Lattice-Matched Heterostructure

Yoshitaka Taniyasu, Jean-François Carlin*, Antonino Castiglia*,
 Raphaël Butté*, and Nicolas Grandjean*
 Materials Science Laboratory,
 *Ecole Polytechnique Fédérale de Lausanne

Among III-nitride semiconductors, AlInN is the only ternary alloy that can be grown lattice-matched to GaN at an In composition of 17 % [1]. Lattice-matched AlInN/GaN heterostructures should be free from cracks, strain-driven composition inhomogeneities, and strain-related defects, which are limiting the performance of ultraviolet/visible light-emitting diodes (LEDs) and laser diodes (LDs) when using conventional lattice-mismatched AlGaIn/GaN or InGaIn/GaN heterostructures. In addition, an AlInN/GaN structure has a large bandgap discontinuity and a large refractive index contrast even at the lattice-matched condition [1], which leads to strong carrier and optical confinements. Thus, AlInN/GaN structures are expected not only to improve the device properties but also to increase the design flexibility for novel III-nitride devices.

Doping control of AlInN lattice-matched to GaN is crucial for device applications. However, non-intentionally doped AlInN has so far shown n-type conduction with high residual donor concentration, which is a significant obstacle to p-type doping as well as to intentional n-type doping. To reduce the residual donor concentration, we grew AlInN under an In-rich condition to benefit from the In surfactant effect. Then, n-type conduction of AlInN was intentionally controlled by Si doping. On the other hand, we found that one of the compensating defects for p-type doping is related to the presence of surface pits. By decreasing the pit density, p-type AlInN was successfully obtained by Mg doping (Fig. 1) [2].

Using p-type AlInN, we fabricated InGaIn/GaN multiple quantum wells (MQWs) LEDs. The LEDs show light emission at a wavelength of 445 nm, which corresponds to electron-hole recombinations occurring in the InGaIn/GaN MQWs (Fig. 2). This confirms the efficient hole injection from the p-type AlInN layer to the MQWs. The achievement of p-type as well as intentional n-type AlInN will open further new possibilities for III-nitride devices.

[1] J.-F. Carlin and M. Illegems, *Appl. Phys. Lett.* **83** (2003) 668.

[2] Y. Taniyasu, J.-F. Carlin, A. Castiglia, R. Butté, and N. Grandjean, *Appl. Phys. Lett.* **101** (2012) 082113.

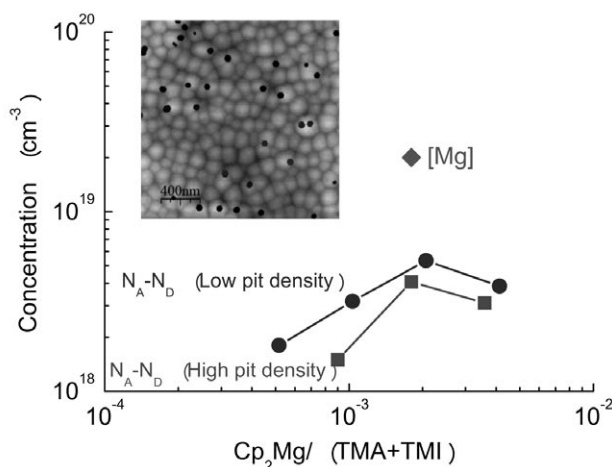


Fig. 1. Net acceptor concentration $N_A - N_D$ of Mg-doped AlInN with high and low pit density as a function of Mg flow rate. Inset: AFM image of AlInN surface.

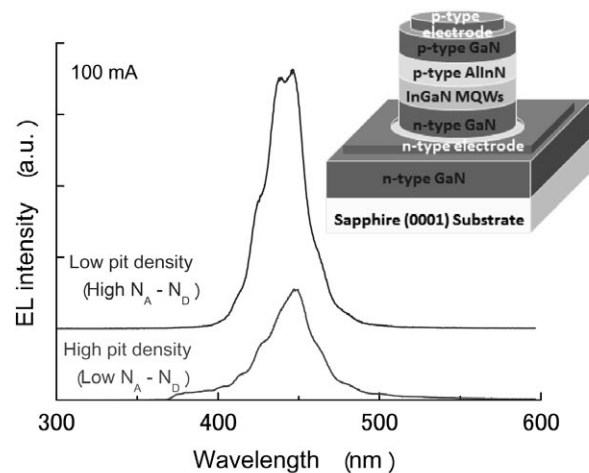


Fig. 2. Electroluminescence of InGaIn/GaN MQW LEDs using p-type Mg-doped AlInN with high and low pit density.

Universal Superconducting Ground State in Nd_2CuO_4 and $\text{Nd}_{1.85}\text{Ce}_{0.15}\text{CuO}_4$

Yoshiharu Krockenberger, Hideki Yamamoto, and Michio Naito*
Materials Science Laboratory, *Tokyo Univ. of Agricul. & Technol.

The induction of superconductivity in electron-doped cuprates is associated to an annealing process, quite in contrast to hole doped cuprates. Hence, while the copper coordination number of hole doped cuprates is five or six, it is four for electron doped cuprates. These four-fold coordinated copper ions form two-dimensional, square-planar CuO_2 plaquettes. So far it has been believed that the superconducting phase diagram of electron and hole doped cuprates is nearly symmetric with respect to doping in antiferromagnetic-insulating and superconducting orders. For the understanding of high temperature superconductivity it was therefore assumed that the ubiquitous insulating state is prerequisite in the absence of doping. Here we show that the existence of an antiferromagnetic- and insulating order for electron doped cuprates is not mandatory but a consequence of the annealing treatment. We applied the so-called "two-step annealing" process to Nd_2CuO_4 for the induction of superconductivity. The plain fact that superconductivity can be induced into insulating Nd_2CuO_4 is currently being scrutinized by several methods. Here, we only focus on the superconducting state itself.

Nd_2CuO_4 (NCO) and $\text{Nd}_{1.85}\text{Ce}_{0.15}\text{CuO}_4$ (NCCO) thin films have been grown by molecular beam epitaxy on (001) SrTiO_3 (STO) substrates. NCCO films were annealed in situ whereas NCO films have been annealed ex situ by two-step annealing procedure [1-4]. Thin films were analyzed by high-resolution reciprocal space mapping at each annealing step. A monotonous decrease in c-axis lengths together with a constant in-plane lattice length are strong indicators for effectively evacuating apical oxygen sites of as-grown NCO and NCCO. The electronic properties of NCO and NCCO are nearly identical, i.e., both are metals and the temperature dependence of the resistivity appears to be Fermi liquid like. The superconducting response with respect to external magnetic field is shown in Fig. 1 for NCO and NCCO. The superconducting transition temperature in the absence of magnetic field as well as the magnetic field dependence shows that in both cases, NCO and NCCO, the superconducting response is quantitatively and qualitatively the same. Such a response can be interpreted as follows: The square-planar coordinated CuO_2 plane is a metal and the additional doping only modulates quantities of band filling rather than a destruction of a long-range antiferromagnetic order.

[1] Y. Krockenberger et al., Phys. Rev. B **85** (2012) 184502.

[2] Y. Krockenberger et al., Jpn. J. Appl. Phys. **51** (2012) 010106.

[3] H. Yamamoto et al., Physica C **470** (2010) 1025.

[4] H. Yamamoto et al., Solid State Commun. **151** (2011) 771.

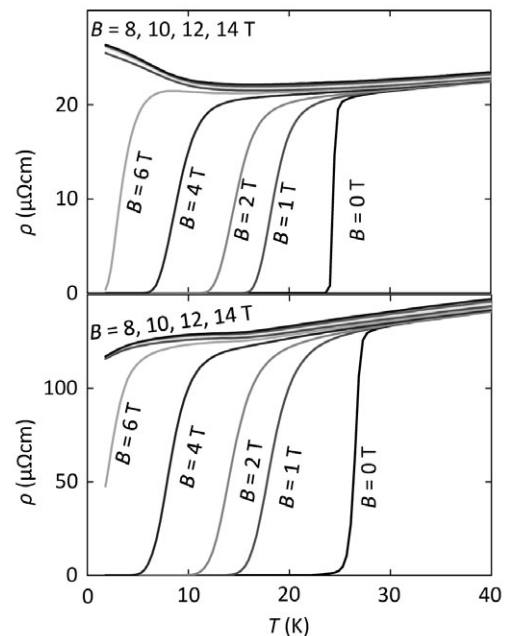


Fig. 1. Resistivity vs temperature of NCCO (top) and NCO (bottom) thin films grown on (001) STO substrates after the annealing process for magnetic fields $B = 0, 1, 2, 4, 6, 8, 10, 12, \text{ and } 14$ T.

Label-Free Protein Detection on Graphene Oxide Surface

Kazuaki Furukawa and Yuko Ueno*

Materials Science Laboratory, *NTT Microsystem Integration Laboratories

Graphene oxide (GO) is an analogue of an oxidized form of graphene, which contains a number of C-O bonds generated by the oxidization of C=C double bonds. GO holds an atomically thin sheet-like structure like graphene, but at the same time it shows many different features from graphene. For instance GO is an insulator, water-dispersive material and efficient fluorescence quencher. We designed and built the label-free protein recognition system on the GO surface using these unique properties [1].

We used GO fixed on a solid surface. The GO surface was modified using pyrene linker to sp^2 domains left in GO and the thrombin aptamer with a probe dye (FAM) bonded at the other terminus (Fig. 1, top). Here the aptamer is a single strand DNA that forms a complex with a specific target molecule. In this study, we used the aptamer for thrombin, an important protein for blood clotting, to demonstrate the idea.

The recognition mechanism is schematically shown in Fig. 1. Fluorescence from the dye is quenched by the GO at the initial stage when the modified molecules adsorbed on the GO surface with the strong interaction between single strand DNA and GO. The fluorescence recovers when the aptamer recognizes and forms a complex with thrombin (Fig. 1, bottom). This is because the dye is separated from the GO surface by the recognition. The validity of the system was confirmed using a single piece of GO. Fluorescence microscope observations showed that the fluorescence recovers only on the GO surface after the thrombin addition (Fig. 2, top). The thickness of GO was increased about 2.9 nm upon the thrombin recognition, which was traced by atomic force microscope observations for the same GO piece (Fig. 2, bottom). The experiments demonstrated the successful label-free detection of thrombin. Our system is advantageous for the operation in microfluidics because the GO piece is firmly fixed on the solid surface. With an increase variety of detectable proteins by choosing different aptamers, it provides a common platform of GO aptasensors.

[1] K. Furukawa et al., *J. Mater. Chem. B* 1 (2013) 1119.

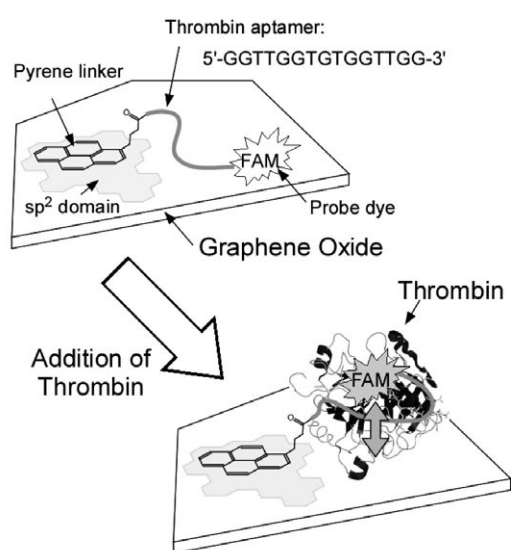


Fig. 1. Schematic drawing of aptamer-modified graphene oxide surface and its molecular detection mechanism.

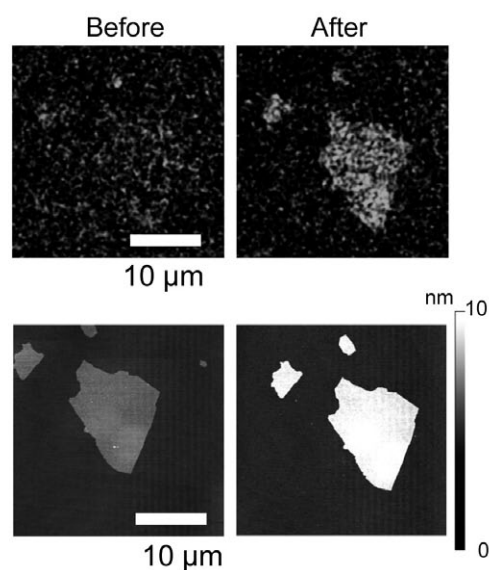


Fig. 2. Fluorescence microscope (top) and atomic force microscope (bottom) images of a GO piece before and after thrombin addition.

Epitaxial Trilayer Graphene Mechanical Resonators Obtained by Electrochemical Etching Combined with Hydrogen Intercalation

Makoto Takamura, Kazuaki Furukawa, Hajime Okamoto*,
Shinich Tanabe, Hiroshi Yamaguchi*, and Hiroki Hibino
Materials Science Laboratory, *Physical Science Laboratory

Graphene is an ideal material for use in nano-electromechanical systems due to its low mass density and exceptional mechanical properties, such as its high Young's modulus. The fundamental mechanical resonance properties of graphene resonators are now being investigated using systems fabricated from monolayer exfoliated graphene flakes. Exfoliation is a simple way of producing high-quality graphene flakes, but it does not provide good control of the shape and thickness of the graphene. Consequently, there have been few studies on bilayer and trilayer graphene resonators. In this article, we report the creation of trilayer epitaxial graphene resonators through strict control of the number of layers and their mechanical resonance properties.

In this study, we created trilayer epitaxial graphene resonators by using bilayer graphene epitaxially grown on SiC(0001) substrate as a starting material [1]. The epitaxial growth method creates a buffer layer, where carbon atoms are partially bound to silicon atoms of the substrate. To make the buffer layer into a graphene layer, we decoupled the Si-C bonds by hydrogen intercalation and performed electrochemical wet etching of the SiC substrate. These procedures allow us to control the number of layers precisely. A scanning electron microscopy (SEM) image [Fig. 1(a)] verifies that the double-clamp graphene beam is suspended between the Au/Cr pads. A cross-sectional transmission electron microscope (TEM) image [Fig. 1(b)] shows that the suspended graphene is trilayer. We can thus conclude that the buffer layer and the bilayer graphene turned into trilayer graphene. We next investigated mechanical resonance properties of the trilayer graphene. The amplitude-versus-frequency curve for the trilayer graphene resonator (Fig. 2) shows the resonant frequency (f_0) to be 7.52 MHz and the quality factor to be ~ 600 at room temperature in a vacuum of 10^{-5} Pa. However, we calculated f_0 to be 0.4 MHz on the basis of standard beam theory. Another SEM image showed that the resonator has a buckled-shape deformation. This enhances the stiffness of the resonator, and as a result, f_0 was higher than expected. The inverse of the quality factor, Q^{-1} , of the trilayer graphene showed the typical temperature dependence of monolayer graphene with a doubly clamped structure. This implies that doubly clamped graphene resonators have a common mechanism of energy loss irrespective of the number of layers.

[1] M. Takamura et al., *Jpn. J. Appl. Phys.* **52** (2013) 04CH01.

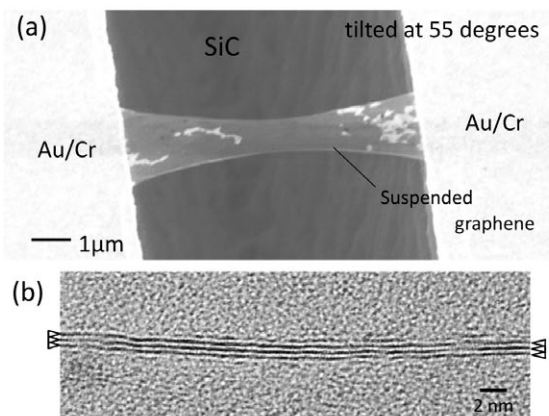


Fig. 1. (a) An SEM image and (b) a cross-sectional TEM image of suspended trilayer graphene.

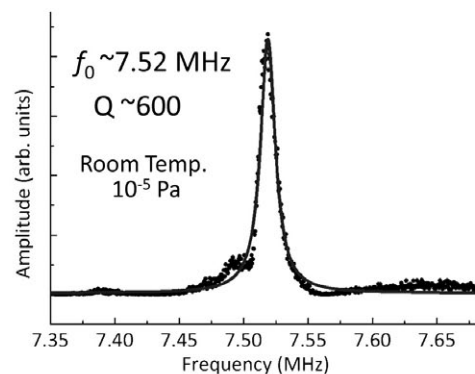


Fig. 2. The amplitude-versus-frequency curve for the trilayer graphene resonator.

Self-Organization of Quasi-Free-Standing Monolayer Graphene Nanoribbon Networks

Yuya Murata, Makoto Takamura, Hiroyuki Kageshima, and Hiroki Hibino
Materials Science Laboratory

Graphene, a two-dimensional (2D) crystalline sheet of carbon, has generated considerable attention owing to its ultrathin geometry and high carrier mobility, with potential application in high-performance low-power electronics. It has been shown that the band gap of graphene can be controlled when it is tailored into a ribbon shape with a width of up to several nanometers [1]. However, methods such as lithography do not satisfy the requirements for the ideal nanoribbons in terms of production efficiency, uniformity of crystal orientation, and edge structure. On the other hand, it has been reported that a buffer layer on a SiC(0001) surface is decoupled from the substrate by H intercalation and it turns into graphene (quasi-free-standing monolayer graphene, QFMLG) [2]. Although the buffer layer is a 2D sheet of carbon like graphene, it is electrically insulating due to covalent bonds with the substrate. It is desirable to desorb H atoms partially and create insulating regions in QFMLG for fabrication of graphene nanostructures. We investigated H desorption from QFMLG and found a self-organization of QFMLG nanoribbon networks during the H desorption process.

We performed in-situ STM observations of the H desorption process on QFMLG. Above 630°C, H-desorbed regions expand from SiC step edges (Fig. 1). Each H-desorbed region increases in size and is split into several patches by QFMLG nanoribbons. Finally, H-desorbed patches separated by the network of QFMLG nanoribbons cover the entire surface. The average width and length of the QFMLG nanoribbons are a few nanometers and ~10 nm, respectively. The nanoribbons run along the SiC[11 $\bar{2}$ 0] directions, with uniform armchair edges. The nanoribbon shows the graphene $\sqrt{3} \times \sqrt{3}$ surface structure, indicating electron scattering at the boundary between the QFMLG and H-desorbed regions (Fig. 2) [3].

[1] M. Y. Han et al., Phys. Rev. Lett. **98** (2007) 206805.

[2] C. Riedl et al., Phys. Rev. Lett. **103** (2009) 246804.

[3] K. Sakai., Phys. Rev. B **81** (2010) 235417.

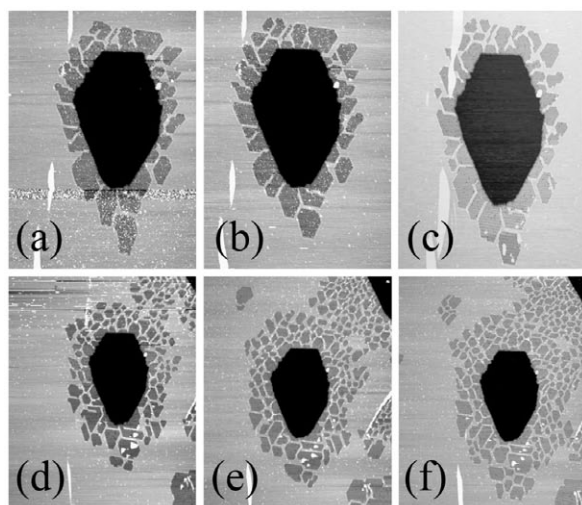


Fig. 1. Series of time-lapse STM images at 590°C, with elapsed time of (a) 0, (b) 10, and (c) 64 min (182 nm \times 250 nm), and at 630°C, with (d) 0, (e) 37, and (f) 69 min (273 nm \times 341 nm).

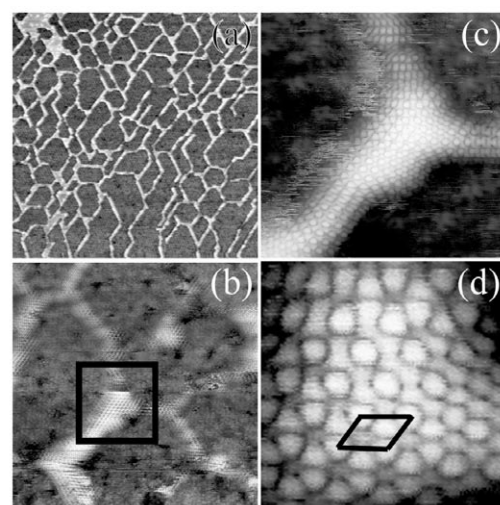


Fig. 2. QFMLG nanoribbon networks (a) 200 nm \times 200 nm, (b) 30 nm \times 30 nm, (c) 10 nm \times 10 nm, (d) 2.5 nm \times 2.5 nm. The rhombus shows a graphene $\sqrt{3} \times \sqrt{3}$ unit cell.

Reconstitution of Homomeric GluA2 Receptors in Supported Lipid Membranes: Functional and Structural Properties

Jelena Baranovic, Chandra S. Ramanujan, and Nahoko Kasai*
University of Oxford, *Materials Science Laboratory

Alpha-amino-3-hydroxy-5-methyl-4-isoxazole propionic acid receptors (AMPA receptors) are glutamate-gated ion channels ubiquitous in the central nervous system where they mediate fast excitatory neurotransmission, and act as molecular determinants of memory formation and learning. Structural studies of full-length AMPARs by electron microscopy (EM) and X-ray crystallography have provided important insights into channel assembly and function. However, the correlation between structure and functional states of the channel remains ambiguous, particularly since these functional states can only be assessed with the receptor bound within an intact lipid bilayer. Our group demonstrated structural examination of reconstituted functioning GluA3 by using atomic force microscopy (AFM) [1], however, the reason why the observed protein height was smaller than that observed by EM was still unknown.

In this study, to provide a basis for investigating AMPAR structure in a membrane environment, we developed an optimized reconstitution protocol of GluR2 whose structure has previously been characterized by EM, and examined their function and structure [2]. AFM studies of the reconstituted samples provide high-resolution images of full-length membrane-embedded AMPARs at densities comparable to those in postsynaptic membranes (Fig.1). Single-channel recordings of reconstituted GluA2 recapitulate key electrophysiological parameters of the channels expressed in native cellular membranes (Fig.2). The data demonstrate the effect of protein density on conformational flexibility and dimensions of the receptors and provide the first structural characterization of functional, membrane-embedded AMPARs, thus, laying the foundation for correlated structure-function analyses of the predominant mediators of excitatory synaptic signals in the brain.

[1] N. Kasai et al., *BBA General Subjects* **1800** (2010) 655.

[2] J. Baranovic, C. S. Ramanujan, and N. Kasai, *J. Biol. Chem.* **288** (2013) 8647.

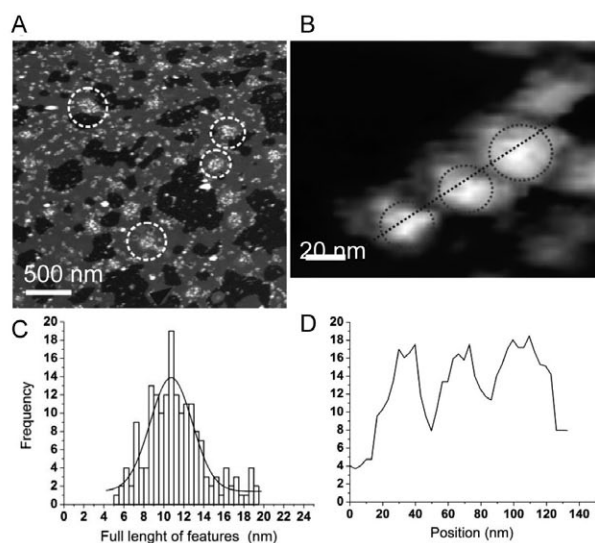


Fig. 1. AFM image of GluA2 reconstituted at high density (A) and zoom of a GluA2 cluster composed of three proteins (B). Height histogram of GluA2 reconstituted at high density (C), and a height profile of a dotted line in B (D).

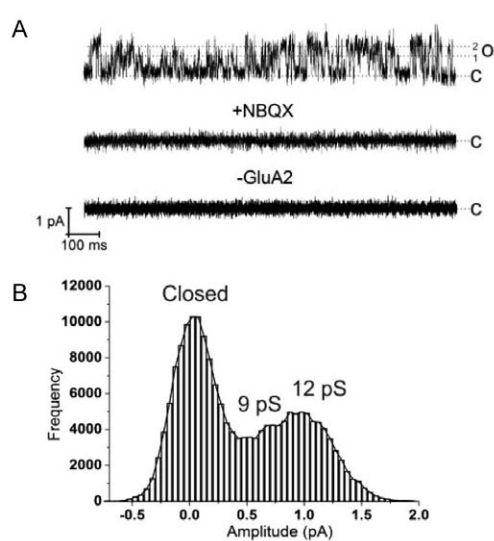


Fig. 2. Activity of reconstituted GluA2. (A) Single-channel current at +80 mV in 5 mM L-Glu and 250 μ M CTZ; the signal was absent in the presence of NBQX (middle trace) and in the negative control (bottom trace). (B) Single-channel conductance at +80 mV with a Gaussian fit.

Electrostatic Control of Artificial Cell Membrane Spreading by Tuning the Thickness of an Electric Double Layer in a Nanogap

Yoshiaki Kashimura and Kazuaki Furukawa
Materials Science Laboratory

We have reported that the self-spreading of an artificial cell membrane (ACM) on a solid support could be controlled electrostatically by modulating an electric field applied between nanogap electrodes, where we concluded that the electric double layer played a significant role in the trap of the ACM [1]. In this study, we describe the mechanism of the electrostatic control of ACM self-spreading, and investigate the dependence of the ionic concentration of an electrolyte and the nanogap spacing under finely controlled conditions [2].

A lipid mixture (molar ratio 7:3) consisting of uncharged L- α -phosphatidylcholine and negatively charged L- α -phosphatidylglycerol containing 1 mol% Texas Red-DHPE was prepared. A small amount of the solid was attached to the device. The self-spreading of an ACM was initiated by immersing the device in an electrolyte solution including 1-100 mM NaCl. A DC voltage (-50 mV) was applied between nanogap electrodes during operation.

We calculated the electric potentials in the nanogap as a function of the distance from one side of the electrode surfaces as shown in Fig. 1. When the nanogap spacing (d) is sufficiently larger than the thickness of the electric double layer (D), the electric field is shielded by counterions in an electrolyte solution leading to no voltage-dependent change in self-spreading [Fig. 1(a)]. In contrast, when $d \leq 5D$, the electric field can be effectively applied in the nanogap spacing, leading to the electrostatic trapping of the ACM [Fig. 1(b, c)]. We performed experiments to determine whether ACM self-spreading could be controlled at each ionic concentration of NaCl (c) as a function of nanogap spacing. For NaCl solutions, the thickness of the electric double layer is expressed as $D \sim 0.304 / \sqrt{c}$. The results are summarized in Fig. 2. The circles and triangles, respectively, show cases where self-spreading could and could not be controlled by applying a voltage. This result is suggestive of a certain threshold for controlling the self-spreading. Therefore, the maximum nanogap width for controlling the self-spreading at a certain ionic concentration is given by $d_{\max} \sim \alpha D \sim 0.304\alpha / \sqrt{c}$, where α is the threshold factor. According to the above equation, dotted lines with a slope of -0.5 were drawn in Fig. 2 for each α value and the line for $\alpha = 5.5$ provided the best fit with the experiments. This is in good agreement with the prediction obtained from the electric potential calculation, where $d = 5D$ is a threshold for the control of ACM self-spreading, suggesting the validity of our proposed mechanism.

[1] Y. Kashimura et al., J. Am. Chem. Soc. **133** (2011) 6118.

[2] Y. Kashimura et al., IEICE TRANS. ELECTRON **96-C** (2013) 344.

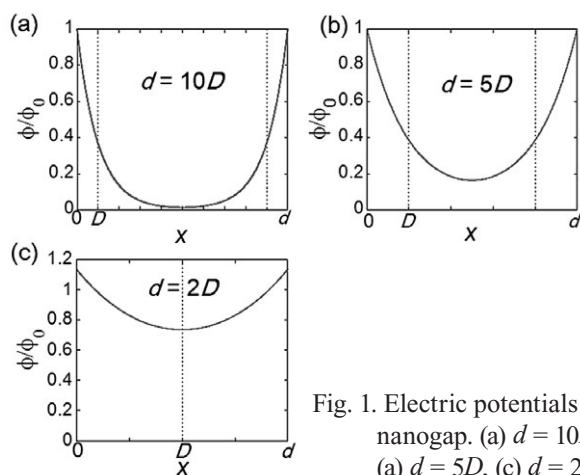


Fig. 1. Electric potentials in the nanogap. (a) $d = 10D$, (b) $d = 5D$, (c) $d = 2D$.

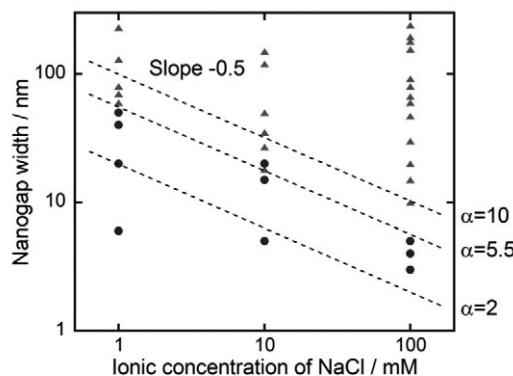


Fig. 2. Result showing whether ACM self-spreading could be controlled at various ionic concentrations. The dotted lines exhibit a slope of -0.5 with various α values.

Conductive Polymer Combined Wearable Electrodes for Electrocardiography Recordings

Shingo Tsukada, Hiroshi Nakashima, Nahoko Kasai, Keiichi Torimitsu,
and Koji Sumitomo
Materials Science Laboratory

In today's aging society, the continuous monitoring of the heartbeat and electrocardiograms is expected to reduce the risk of a heart attack (sudden death) through the early detection and early treatment of any cardiac malfunction. Monitoring is also effective in preventing the physical overload caused by improper exercise and the accumulation of mental stress. However, conventional biomedical electrodes use an electrolyte paste or gel, which results in excessive wetting of the skin surface and occasionally causes skin irritation or contact dermatitis. The conductive polymer (PEDOT-PSS) coated silk or synthetic fibers have been used to fabricate wearable electrodes to obtain biomedical recordings [1]. The new bioelectrode made of conductive fiber is flexible, biocompatible, and hydrophilic and thus allows stable recording of bioelectric signals equivalent to that of a conventional electrode, without using any electrolyte paste or gel. Experiments on human volunteers (10 able-bodied people) wearing undershirts equipped with the electrode (Fig. 1) revealed successful long-term recording of the heartbeat and electrocardiograms (Fig. 2) [2]. Based on this result, the heartbeat and electrocardiograms can be monitored continuously simply by wearing the electrode shirts. We can expect the electrode to find various applications in sports, health enhancement, and the support of medical diagnosis, as well as scientific research.

[1] S. Tsukada, H. Nakashima and K. Torimitsu, PLoS ONE **7(4)** (2012) e33689.

[2] 2013 Feb 12 NTT Press release.

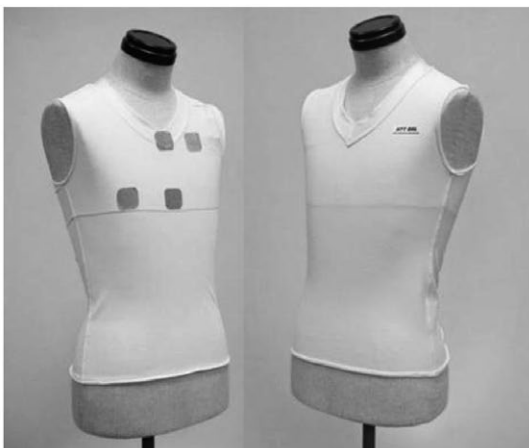


Fig. 1. A wearable electrode has been fabricated by mounting a conductive textile on a shirt.

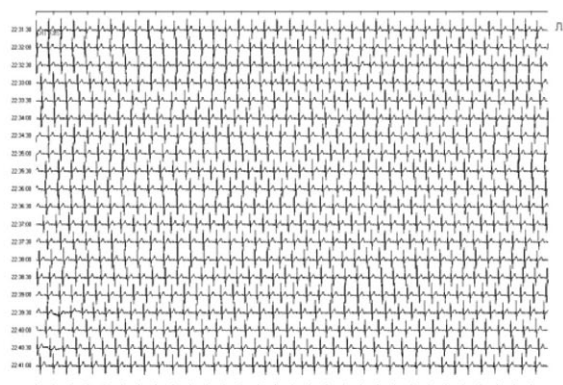


Fig. 2. Simply wearing the shirt enables the Holter electrocardiograms to be monitored.

Donor-Based Single Electron Pump

Gabriel P. Lansbergen, Yukinori Ono, and Akira Fujiwara
Physical Science Laboratory

Down scaling of semiconductor devices has been providing us the opportunity to explore a new approach to devices with a limited amount of dopants in the active device area, whose functionality is based on individual dopants. Recent progress in nanofabrication has led to the observation of the charge of a single dopant in silicon nanotransistors [1] and the operation of a single-atom electron spin qubit in silicon [2].

Recently we have investigated a novel device concept based on single dopant functionality, that is, we have demonstrated multiple-donor based single electron pumps [3]. Our devices consist of Si nanowire MOSFETs in series fabricated on a silicon-on-insulator (SOI) wafer (see Fig. 1). A stacked gate layer structure is employed; the lower layer consists of three fine gates, LG (not used), MG, and RG, defined by electron beam lithography, and the top layer consists of a large single upper gate (UG). Donor atoms (arsenic) are locally implanted in the nanowire channel between MG and RG using a 60 nm wide aperture in a resist mask. For charge transfer operation (see Fig. 1 right), we apply an AC signal with a frequency f to MG. RG is tuned such that it induces a small barrier in the Si nanowire beneath it. When the barrier formed by V_{MG} is in its low state (I), electrons enter from the source. When the barrier is subsequently ramped up (II) to its high state (III) by V_{MG} , electrons are captured at donor sites, and then the gate electric field ionizes the donors and evacuates their bound electrons to the drain region. Figure 2 shows the charge pump characteristics I_{SD} versus V_{UG} at various right fine gate voltages (V_{RG}). Current plateaus due to single-electron transfer via multiple dopants are clearly observed. It is also shown that the number of dopants is tunable by V_{RG} ; positively increased V_{RG} reduces a depletion region in the island, making more donors available for charge transfer. Temperature-dependent characterization allows us to extract the ionization energy of a single arsenic donor. Dopant based SE pumps are capable of pumping multiple electrons with the number of dopants and therefore promising for electrical standards generating high currents.

[1] Y. Ono et al., Appl. Phys. Lett. **90** (2007) 102106.

[2] J. J. Pla et al., Nature **489** (2012) 541.

[3] G. P. Lansbergen, Y. Ono, and A. Fujiwara, Nano Lett. **12** (2012) 763.

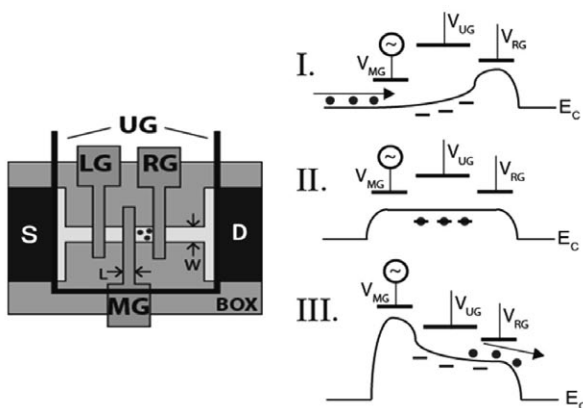


Fig. 1. (Left) Schematic top view of Si nanowire MOSFET ($W = 80$ nm, $L = 100$ nm). (Right) Potential diagram of operation of charge pump.

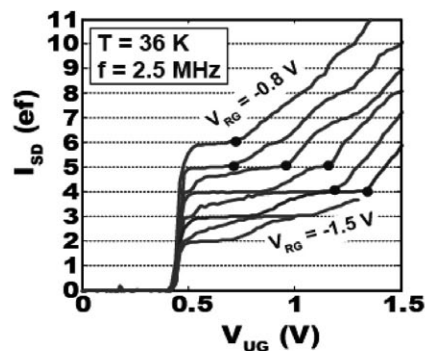


Fig. 2. Pump current as a function of gate voltage, showing single-electron transfer via a tunable number of individual donors up to $I = 6ef$.

Signal Detection Via a Transistor with Steep Current Characteristics

Katsuhiko Nishiguchi and Akira Fujiwara
Physical Science Laboratory

A field-effect transistor (FET) is a device to amplify signals applied to a gate terminal, which can be used for a sensor with a high charge sensitivity. To maximize the sensitivity, current characteristics as a function of gate voltage should be as steep and as non-linear as possible. However, steepness or subthreshold swing (SS) of current characteristics is fundamentally limited by thermal fluctuation, e.g., 60 mV/dec at room temperature. On the other hand, practical use of the sensor necessitates suppression of outside noise masking an output signal from the FET. In this work, we demonstrate detection of a signal buried in noise with a transistor having extremely small SS [1].

The device is composed of a wire channel covered with three gates as shown in Fig. 1 [2]. An upper gate (UG) and back gate (BG) is used to induce a source and drain electrically. Then, current is modulated by a lower gate (UG) as in a conventional LG. When drain voltage is large enough to induce hot electrons, they generate electron-hole pairs due to impact ionization. Generated holes flow in a body region of the channel and thus amplify electron current, which lead to further impact ionization. This positive feedback makes current characteristics steeper and SS reaches ~ 1 mV/dec regardless of thermal fluctuation (Fig. 2).

Detection of signal buried in noise is performed by using stochastic resonance (SR), which is a unique phenomenon that takes advantage of noise to enhance the response of a system to a weak signal [3]. Non-linear current characteristics of the FET enable SR to provide a correlation between the noise-buried input and output current signals. It is confirmed experimentally and theoretically that stronger non-linearity, i.e., small SS, and bistability of current characteristics boost an effect of SR (Fig. 3). Moreover, the dynamic bistability enables SR effect to be enhanced by adding common noise to multiple FETs. The FET providing such unique characteristics opens the way to use SR for practical applications.

This work was partly supported by the Funding Program for Next Generation World-Leading Researchers of JSPS (GR103)

- [1] K. Nishiguchi and A. Fujiwara, *Appl. Phys. Lett.* **101** (2012) 193108.
- [2] K. Nishiguchi and A. Fujiwara, *Appl. Phys. Express* **5** (2012) 085002.
- [3] L. Gammaitoni et al., *Rev. Mod. Phys.* **70** (1998) 223.

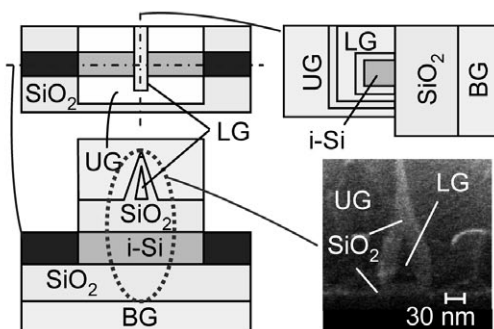


Fig. 1. Cross-sectional views and SEM image of the device.

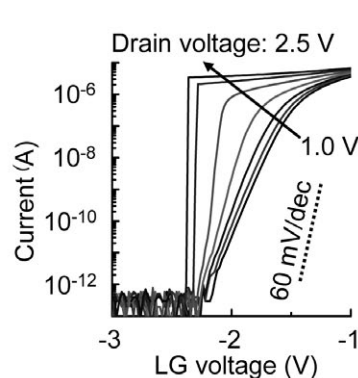


Fig. 2. Current-voltage characteristics.

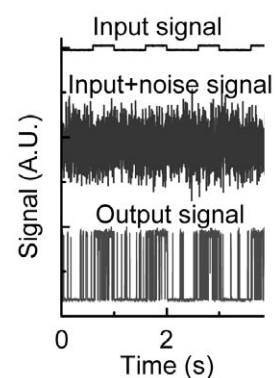


Fig. 3. Detection of a signal buried in noise.

Cavity-Electromechanics with Phonons

Imran Mahboob, Katsuhiko Nishiguchi, Hajime Okamoto, and Hiroshi Yamaguchi
Physical Science Laboratory

Cavity-opto/electromechanical systems exploit the parametric coupling between a photonic cavity and a mechanical resonator [1]. The parametric coupling arises from the motion of the mechanical element that can modulate the cavity's frequency. This results in the emergence of side-bands at the sum (blue) and difference (red) frequency of the constituent resonators. By optically pumping on the side-bands, the coupling between the two systems can be enhanced. This in turn can induce an EIT-like transparency in the cavity where energy is transferred to the mechanical resonator. Alternatively, the cavity can also manipulate the oscillation dynamics of the mechanical resonator and even cool it into its quantum ground state i.e. energy is transferred to the cavity from the mechanical resonator.

In this work, we demonstrate an all-phonon analogue of a photonic cavity-opto/electromechanical system where the mechanical oscillation of interest is composed by the 1st oscillation mode and role of the phonon cavity is played by the 2nd oscillation mode. The parametric coupling between the modes is created by modulating the tension in the electromechanical resonator at the sideband frequencies. This in turn modifies the oscillation dynamics of the constituent modes that can drive the parametric coupling between them.

The experiments were performed in a piezoelectrically active GaAs/AlGaAs electromechanical resonator which sustained the 1st and 2nd modes at 171.3 kHz and 470.9 kHz respectively (Fig. 1). The piezoelectric transducer enabled the tension in the mechanical resonator to be modulated at the sidebands. The creation of parametric coupling is demonstrated by probing the 2nd mode whilst pumping on the red-side band (see Fig. 2). This results in energy from the 2nd mode being transferred to the 1st mode. As the pump amplitude is increased, the coupling between modes is made so strong that it results in parametric normal mode splitting where the modes are no longer distinct but rather a hybrid. We exploit the dynamic nature of this parametric coupling to create a transparency in the phonon cavity and to cool the 1st mode [2].

[1] T. Kippenberg and K. Vahala, *Science* **321** (2008) 1172.

[2] I. Mahboob et al., *Nature Physics* **8** (2012) 387.

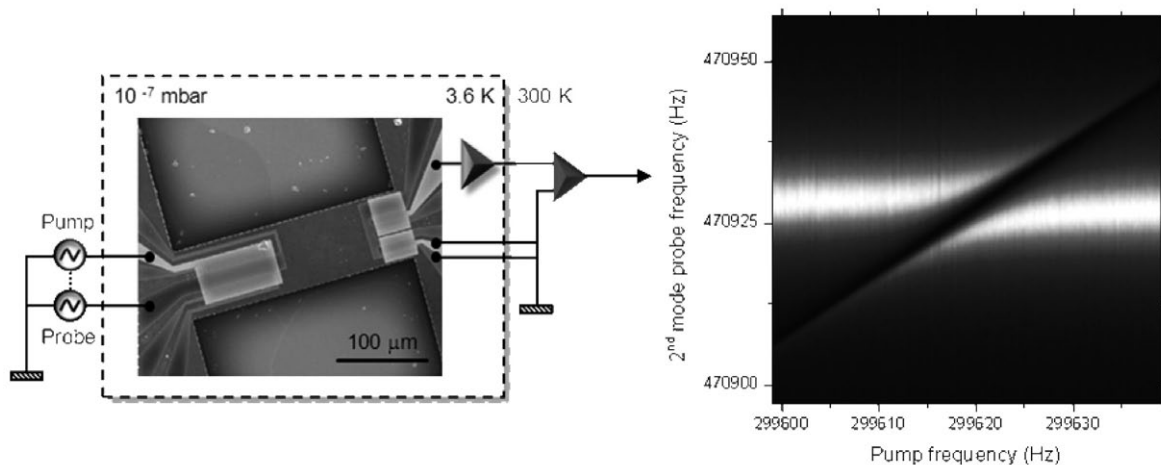


Fig. 1. An SEM image of the electromechanical resonator and simple circuit schematic.

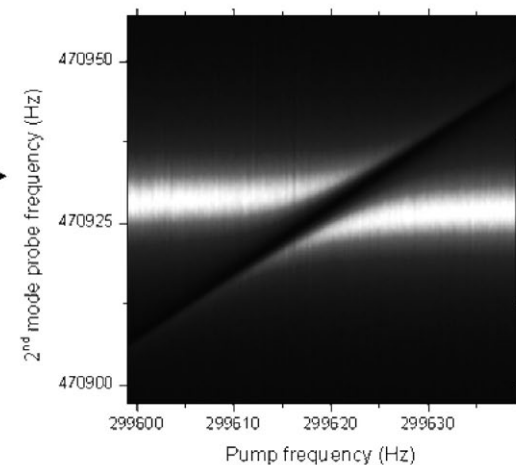


Fig. 2. The 2nd mode being probed at large red-pump amplitudes which undergoes parametric normal mode splitting indicating that it is strongly coupled to the 1st mode.

Ferromagnetic-Induced Component in Piezoresistance of GaMnAs

Koji Onomitsu^{1,2}, Imran Mahboob¹, Hajime Okamoto¹, Yoshiharu Krockenberger²,
and Hiroshi Yamaguchi¹

¹Physical Science Laboratory, ²Materials Science Laboratory

The piezoresistive effect (PR) is defined as the change in resistance of a material due to an applied stress and is a fundamental property of semiconductors and metals. In conventional semiconductors, PR originates from a change in either carrier density or mobility. PR can also be observed in metals, including ferromagnetic materials, due to geometrical effects. PR provides a powerful tool for the investigation of electronic transport properties and can be used for sensing applications. In this study, we report a new mechanism of PR in GaMnAs where the ferromagnetic ordering plays an essential role. We characterized PR by incorporating a GaMnAs piezoresistor into a micromechanical cantilever and investigated its temperature and magnetic field dependence at the ferromagnetic transition. A clear ferromagnetic-induced piezoresistance component (FMPR) was found below the Curie temperature (T_c) of our GaMnAs ($T_c \sim 48$ K). Figure 1 shows the schematic illustration of the cantilever together with electrode on PZT and measurements setup. The frequency response of PR is detected via down-mixing technique. The reference frequency can be tuned by adjusting bias-current frequency (f_1) and actuation frequency (f_2). Figure 2 shows the temperature dependence of PR around T_c without external magnetic field: (a) real part and (b) imaginary part. Data (dots) show the measured frequency response, and the straight lines were obtained by calculations. Data and calculated lines have been offset by $\Delta = 0.04 \Omega$ for clarity.

These results indicate that the FMPR of GaMnAs arises from the perturbation of spontaneous spin ordering by the applied strain. Moreover, the change in resistance is delayed with respect to mechanical strain. We deduced a delay time of 230 ± 35 ns. The experimental results presented indicate that the micromechanical method of characterizing spin dynamics is complementary to conventional electrical and optical methods [1].

[1] K. Onomitsu et al., Phys. Rev. B **87** (2013) 060410 (R).

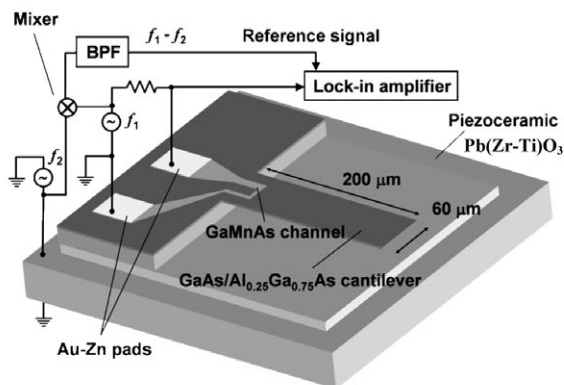


Fig. 1. Schematic illustration of the cantilever on PZT and measurements setup.

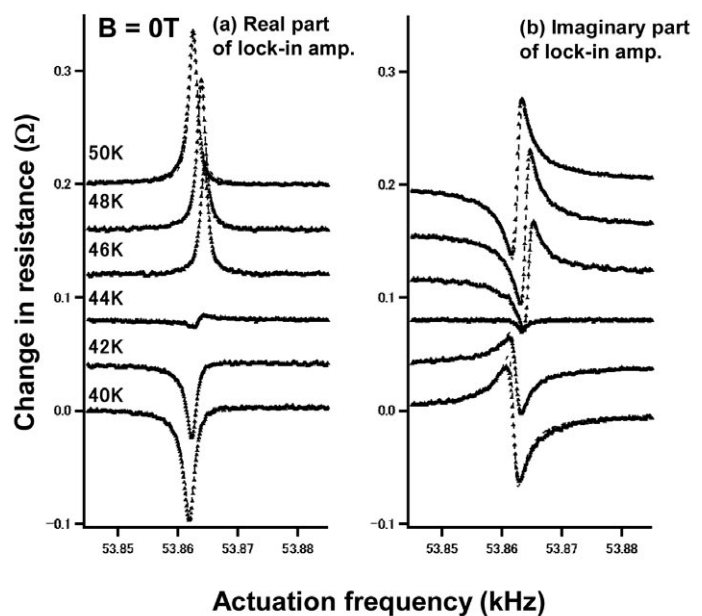


Fig. 2. Temperature dependence of PR around T_c .

An Electromechanical Membrane Resonator

Daiki Hatanaka, Imran Mahboob, Hajime Okamoto, Koji Onomitsu, and Hiroshi Yamaguchi
Physical Science Laboratory

Membrane-based mechanical resonators (MMR) have received much interest because they have high quality-factors [1]. In addition, they also have a large surface area that not only makes them easier to use in optical architectures, but also it makes them more responsive as detectors. However, to date most MMRs have been passive structures with only optical control. The lack of electrical control prevents the development of the MMR for more practical applications. Here, we report a GaAs/AlGaAs-based piezoelectric MMR that enables all electrical transduction of the mechanical motion [2].

The MMR consists of GaAs (5 nm) / Al_{0.27}Ga_{0.73}As (95 nm) / *n*-type GaAs (100 nm) heterostructure on an Al_{0.65}Ga_{0.35}As sacrifice layer (3.0 μm). The circular membrane with a diameter of 30 μm was suspended by removing the sacrifice layer through the center hole with hydrofluoric acid as shown in Fig. 1. All measurements in this report were performed in a high vacuum and at room temperature.

Mechanical oscillations were induced by applying an oscillating voltage to electrode A or B due to the piezoelectric effect and the resulting oscillations were detected by measuring the piezovoltage generated from electrode C. In order to demonstrate its electromechanical functionality, a mechanical logic gate is built with the fundamental (0, 1) mode in the MMR. In the experiment, electrodes A and B are used for binary inputs and electrode C is used for a binary output where electrodes A and C are along the $[\bar{1}\bar{1}0]$ orientation and electrode B is along the $[\bar{1}10]$ orientation as shown in Fig. 1. An excitation of the (0, 1) mode via input A or B results in membrane oscillations with opposite phase due to the opposite sign of the piezoelectric constants in the $[\bar{1}\bar{1}0]$ and $[\bar{1}10]$ orientations in AlGaAs. Therefore, when an actuation of the same magnitude is simultaneously applied to both inputs A and B, mechanical oscillations can be cancelled out, resulting in no piezovoltage at output C. This response from the (0, 1) mode enables the MMR to implement an XOR ($A \oplus B$) logic gate as shown in Fig. 2. Furthermore, we can also demonstrate an OR ($A \cup B$) logic gate in the first (1, 1) mode using a similar method. Thus, the electrically-active MMR promises functions and performance beyond conventional passive MMRs which could be used to develop a broad range of applications for mechanical resonators.

[1] J. D. Thompson et al., Nature **452** (2008) 72.

[2] D. Hatanaka et al., Appl. Phys. Lett. **101** (2012) 063102.

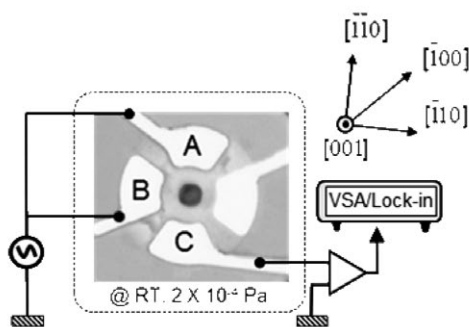


Fig. 1. The piezoelectric MMR and its measurement set-up.

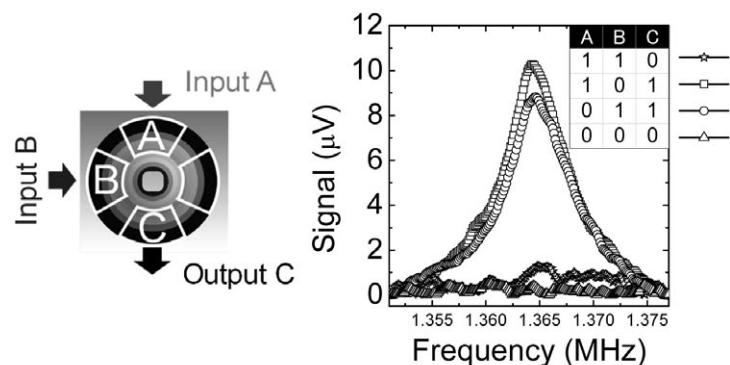


Fig. 2. An XOR logic gate ($A \oplus B$) in the (0, 1) mode.

Shot Noise Spectroscopy on a Semiconductor Quantum Dot in the Elastic and Inelastic Cotunneling Regimes

Yuma Okazaki^{1,2}, Satoshi Sasaki^{1,2}, and Koji Muraki¹
¹Physical Science Laboratory, ²Tohoku University

Shot noise is a time-dependent current fluctuation reflecting the discreteness of charge carriers. Measurements of shot noise in coherent conductors such as a quantum dot (QD) are expected to reveal dynamical mechanisms and underlying correlation in electron transport. Electron cotunneling is a higher-order tunneling process observed in the Coulomb blockade regime. Cotunneling is classified into elastic and inelastic processes; the former involves only the QD ground state, while the latter accompanies dynamical charge fluctuation between the ground and excited states. Shot noise measurements have been reported only for the inelastic cotunneling regime in a carbon nanotube QD [1]. For semiconductor QDs, on the other hand, shot noise measurements in the cotunneling regime are made more challenging by the even lower cotunneling current inherent to semiconductor QDs [2].

Here we study the shot noise in a semiconductor QD in the cotunneling regime. We fabricate a small QD [Fig. 1(a)], in which the level spacing ΔE can be increased up to 1 meV. Owing to this large ΔE , we can obtain cotunneling current high enough as compared to the resolution of our noise measurement setup. Figure 1(b) shows the conductance G as a function of source drain bias V_{sd} . For a small bias range ($|V_{sd}| < 1$ mV), we find small but finite conductance due to elastic cotunneling. For a large bias range ($|V_{sd}| > 1$ mV), on the other hand, G is strongly enhanced due to the strong inelastic cotunneling. Figure 1(c) shows the Fano factor F , which is determined from the measured current noise S_{out} and current I [$F = S_{out} / 2eI$ with e being the electron charge]. We observe the Poissonian Fano factor $F \sim 1$ in the elastic cotunneling regime. On the other hand, we observe an enhancement of the Fano factor up to $F \sim 2.5$ (super-Poissonian Fano factor) in the inelastic cotunneling regime. This large Fano factor results from the fact that the inelastic cotunneling is accompanied by an emission of excess electrons, which leads to electron bunching and enhances the shot noise [3]. The observed difference in the value of the Fano factor can be utilized as a new spectroscopic measurement, by which we can quantitatively distinguish the microscopic origins of charge transport.

[1] E. Onac et al., Phys. Rev. Lett. **96** (2006) 026803.

[2] S. Gustavsson et al., Phys. Rev. B **78** (2008) 155309.

[3] Y. Okazaki, S. Sasaki, and K. Muraki, Phys. Rev. B **87** (2013) 041302(R).

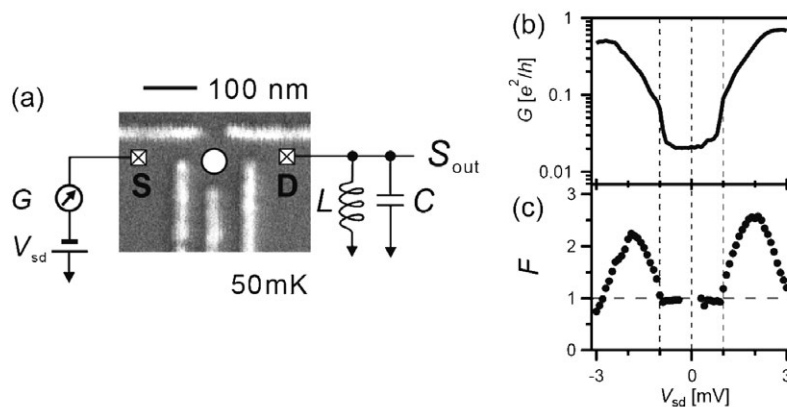


Fig. 1. (a) Device and the setup. The current noise is fed to the LC resonator, and is measured using cold-amplifier. (b) Conductance G and (c) Fano factor F as a function of V_{sd} .

Plasmon Transport in Graphene Investigated by Time-Resolved Electrical Measurements

Norio Kumada, Shinichi Tanabe, Hiroki Hibino, Hiroshi Kamata*, Masayuki Hashisaka*, Koji Muraki, and Toshimasa Fujisawa*
Physical Science Laboratory, *Tokyo Institute of Technology

Plasmons, which are collective charge oscillations, could provide a means of confining electromagnetic field to nanoscale regions. Recently, plasmonics in graphene have attracted interest, particularly because of the tunable plasmon dispersion. In this work, we carried out time-resolved electrical measurements of edge magnetoplasmons (EMPs), which are plasmons localized at graphene edge in a high magnetic field, and demonstrate that the velocity of EMPs can be controlled over two orders of magnitude [1].

Graphene used was grown on SiC substrate. We used two samples, one with and the other without a large top gate. All measurements were carried out at 1.5 K. Plasmons are injected into graphene by applying a voltage step to the injection gate and detected through the detector Ohmic contact fabricated 1.1 mm away from the injection gate [Fig. 1(a)]. From the time of flight between the injector and the detector, the plasmon velocity is determined. In the ungated sample, as the magnetic field is increased, the velocity decreases from 6000 km/s to 2000 km/s [Fig. 1(b)]. In the gated sample, on the other hand, the velocity is about 100 km/s, which is one order of magnitude smaller than that in the ungated sample [Fig. 1(c)]. The smaller velocity is due to the gate screening effect of the electric field in plasmons. At a fixed magnetic field (12 T), as the gate bias and thus the carrier density are decreased, the velocity decreases to 10 km/s with oscillations. These results indicate that the velocity of plasmons in graphene can be controlled over two orders of magnitude by applying the magnetic field, screening the plasmon electric field with a gate metal, and changing the carrier density. The wide tunability of the plasmon velocity encourages designing graphene nanostructures for plasmonic circuits.

This work was supported by KAKENHI.

[1] N. Kumada et al., Nature Commun. 4 (2013) 1363.

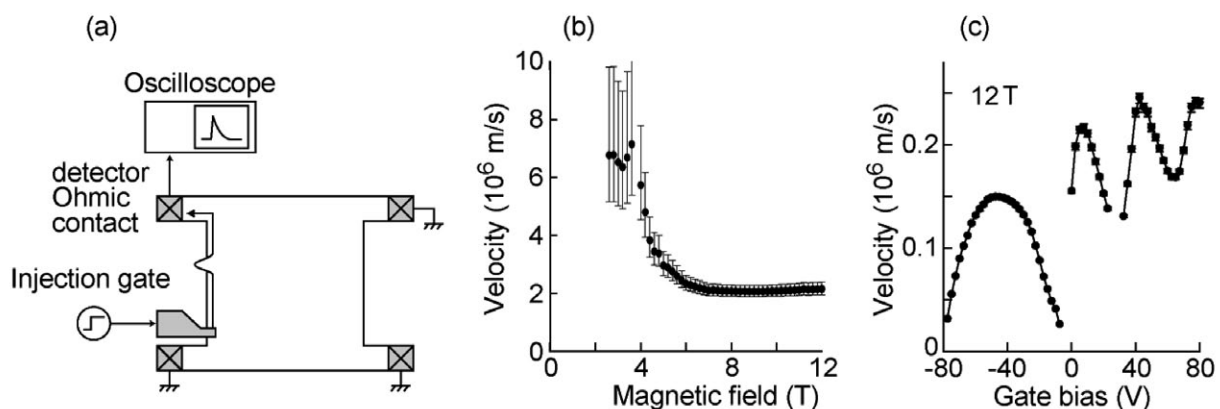


Fig. 1. (a) Sample structure and the experimental setup. (b) Plasmon velocity in the ungated sample as a function of the magnetic field. (c) Plasmon velocity in the gated sample as a function of the gate bias at a magnetic field of 12 T.

Impact of Graphene Quantum Capacitance on Transport Spectroscopy

Keiko Takase, Shinichi Tanabe*, Satoshi Sasaki, Hiroki Hibino*, and Koji Muraki
Physical Science Laboratory, *Materials Science Laboratory

Graphene, a two-dimensional honeycomb lattice of carbon atoms, is known to have the relativistic energy band called Dirac cone. Accordingly, the density of states in graphene depends on the Fermi energy, whereas those in the conventional two-dimensional systems (2DESs) do not rely on the Fermi level. This then indicates that the quantum capacitance, which is defined to be proportional to the density of states, is quite different for graphene and conventional 2DESs. In this study, using a top-gated device fabricated from epitaxial graphene on SiC, we demonstrate that the interplay between quantum capacitances of graphene and interface states in the device changes the appearance of the fan diagram in epitaxial graphene, which consequently represents the relativistic graphene Landau level. This indicates that our transport measurements serve as a kind of energy spectroscopy [1], and thus enables us to deduce the energy broadening of the Landau levels in graphene [1].

The sample is a top-gated Hall-bar device, fabricated from graphene on SiC. At low temperature and low fields, we observe the quantum Hall (QH) state, where the Hall resistance becomes quantized at $h/\{(4N+2)e^2\}$ and longitudinal resistance R_{xx} becomes zero at the Landau level filling factor $\nu = 4N + 2$ (N : integer). The observed QH states are illustrated in a fan diagram [Fig. 1(a)], where R_{xx} is mapped as a function of gate voltage V_g and magnetic field B . At $\nu = 2$, a wide region with zero R_{xx} , indicating the $\nu = 2$ QH state, appears and clear R_{xx} peaks are observed at $\nu = 0, 4$, and 8 . In contrast to the usual case, in which R_{xx} peaks appear as an equidistant linear fan diagram in the $V_g - B$ plane, in our epitaxial graphene device, the trajectories of the R_{xx} peaks are curved and unequally spaced. This can be explained by our model [Fig. 1(c)], in which not only graphene but also the interface states nearby graphene, such as dangling-bond states at SiC or those in the gate insulator, serve as charge reservoirs when V_g is swept. As a result, the quantum capacitance of graphene and that of the interface states associated with the density of states play a significant role in the V_g dependence of the graphene carrier density. Analyzing the V_g dependence with this model allows us to deduce the interface state densities. Furthermore, when the interface state density is much larger than the graphene carrier density, the Fermi level in graphene becomes proportional to V_g . Consequently, R_{xx} peaks in the $V_g - B$ plane represents the graphene Landau-level structure. Filling factor calculated vs. V_g and B in Fig. 1(b) nicely reproduces the experimentally observed peak positions of R_{xx} in Fig. 1(a).

[1] K. Takase et al., Phys. Rev B **86** (2012) 165435.

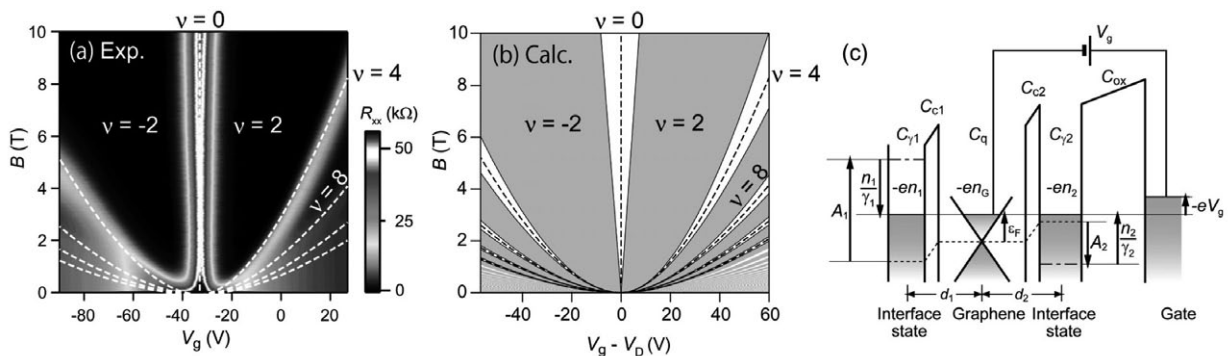


Fig. 1. (a) R_{xx} mapped vs. V_g and B . (b) Filling factors calculated vs. V_g and B . (c) Schematic illustration of the graphene device with nearby interface states.

Energy Relaxation Process of a Quantum Memory Coupled with a Superconducting Qubit

Yuichiro Matsuzaki and Hayato Nakano
Physical Science Laboratory

For quantum information processing, each physical system has a different advantage as regards implementation and so hybrid systems that benefit from the advantage of several systems would provide a promising approach. One common hybrid approach involves combining a superconducting qubit as a controllable qubit and another quantum system with a long coherence time as a memory qubit [1]. The use of a superconducting qubit gives us an excellent controllability of the quantum states and the memory qubit is capable of storing information for a long time. It has been believed that selective coupling can be realized between a superconducting qubit and a memory qubit by tuning the energy splitting between them.

However, we have shown that this detuning approach has a fundamental drawback as regards energy leakage from the memory qubit [2]. Even if the superconducting qubit is effectively separated by reasonable detuning, energy relaxation time in the memory qubit decreases via residual weak coupling when the superconducting qubit is affected by severe dephasing (Fig. 1). This energy transport from the memory qubit to the control qubit can be interpreted as the appearance of the anti Zeno effect induced by the fluctuation in the superconducting qubit. We have suggested possible ways to avoid this energy relaxation process by using decoherence free subspaces, which is feasible with existing technology [2].

This work was supported by KAKENHI.

[1] X. Zhu et al., *Nature* **478** (2011) 221.

[2] Y. Matsuzaki et al., *Phys. Rev. B* **86** (2012) 184501.

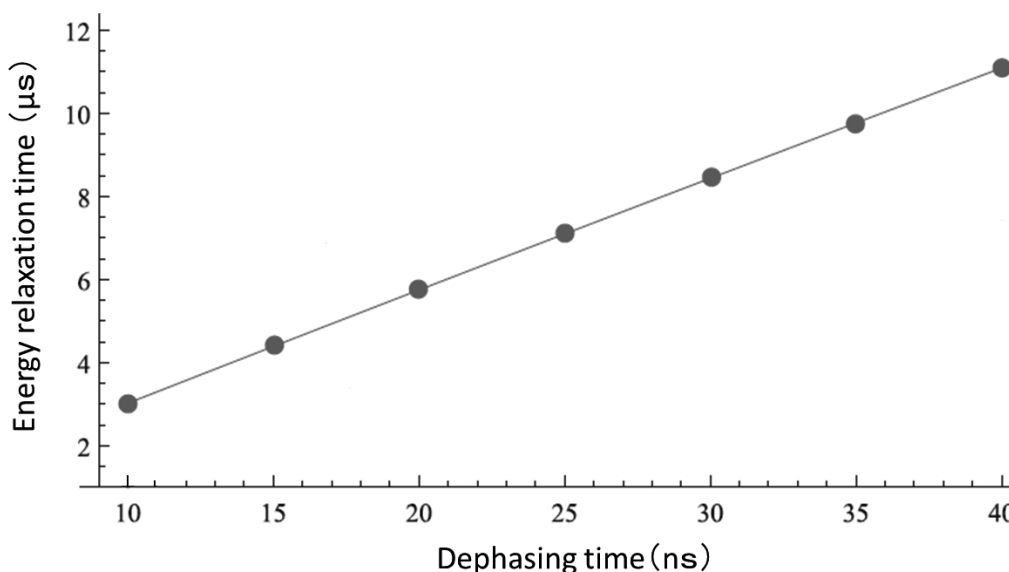


Fig. 1. Relationship between relaxation time of the memory qubit and the dephasing time of the superconducting qubit. We set the coupling strength as 25 MHz and set the detuning energy as 1 GHz.

Evidence of a Crossover from Trions to an Electron-Hole Gas

Masumi Yamaguchi, Shintaro Nomura*, Hiroyuki Tamura, and Tatsushi Akazaki
Physical Science Laboratory, *University of Tsukuba

A trion, the bound state of two electrons and a hole, cross over to the unbound state of the two-dimensional electron gas plus a hole state (2DEG-h) as the excess electron density is increased (see Fig. 1). This is because the Coulomb attraction between the electron and hole is screened by the degenerate 2D electron gas. In studying this crossover, a difficulty lies in the unavoidable spatial disorder of the electrostatic potential existing in samples. In the low-electron-density regime, the electrons are localized at the potential valleys. The electron-density regime where the crossover occurs often overlaps the electron-density regime where the electron localized-delocalized transition occurs.

In this work, we studied the crossover by analyzing the evolution of the PL spectrum using an undoped GaAs QW [1]. Unlike in modulation-doped QWs, which are commonly used for studying 2D electron system, the electron localization occurs at much lower density than the crossover regime since the typical length scale of the disorder potential for our sample is long. Therefore, the electron localization and the crossover are clearly separated in our sample. By measuring the photoluminescence linewidth under perpendicular electric fields, we have traced the variation of the effective radius a^* of the trion as a function of electron density (Fig. 2). The a^* increases sharply above $n_s = 2 \times 10^{14} \text{ m}^{-2}$, at which the screening length drops. Here, the screening length is predicted by nonlinear-screening theory. This is a clear evidence of the trion-2DEG-hole crossover related to the dissociation of the trion state screened by the 2D electron gas.

This work was supported by KAKENHI.

[1] M. Yamaguchi et al., Phys. Rev. B **87** (2013) 081310(R).

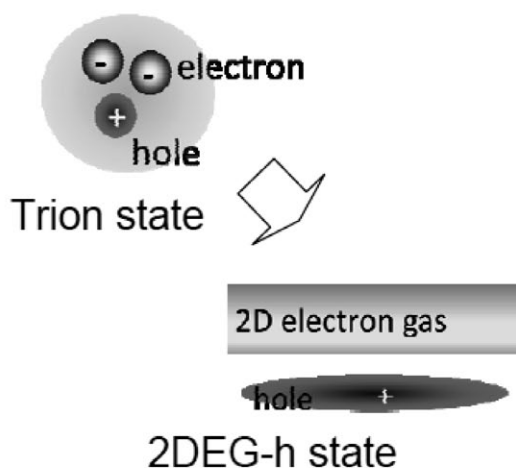


Fig. 1. Trion state and two-dimensional electron gas plus hole state.

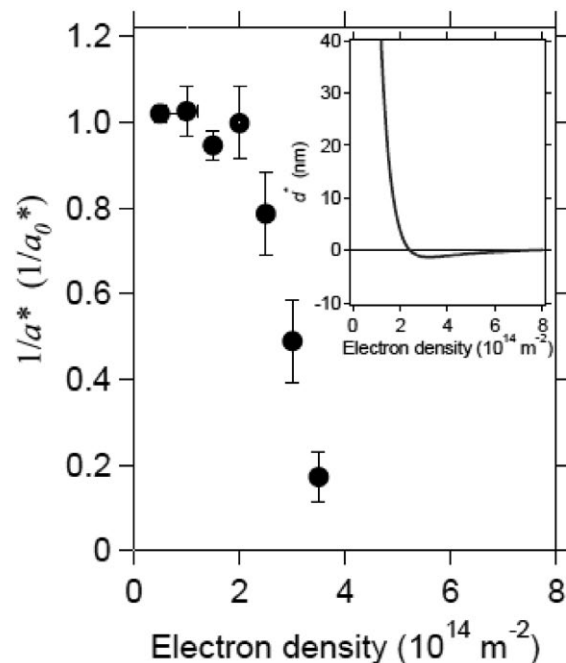


Fig. 2. Electron density dependence of the trion radius a^* . Inset: Screening length.

Fundamental Limit to Qubit Control with Coherent Field

Kazuhiro Igeta
Optical Science Laboratory

Controlling matter qubits with coherent electromagnetic field is regarded as the most promising building block of quantum information processing systems. In practice, we can use the classical field theory which enables us to control a qubit perfectly as described by the Bloch rotation according to the pulse area of the field. However, classical fields exist only as an infinitely strong intensity limit. In reality, strong but finite strength coherent fields are available that will cause control errors because of their lack of infiniteness.

In this work, we formulate the full quantum mechanical interaction between a pure coherent field and a qubit in the general initial state including mixed states. While the fidelity error accompanied by $\pi/2$ pulse control is shown to be inversely proportional to the average photon number in a way similar to that revealed by the former results [1, 2] our results show that the error depends strongly on the initial state of the qubit [3]. Our result (Fig. 1) reveals that the the entanglement built up between the field and the qubit is the origin of the error.

This work was partly supported by CREST of the Japan Science Technology Agency.

- [1] J.Gea-Banacloche, Phys. Rev. A **65** (2002) 022308.
[2] M.Ozawa, Phys. Rev. Lett. **89** (2002) 057902.
[3] K. Igeta, N. Imoto, and M. Koashi, Phys. Rev. A **87** (2013) 022321.

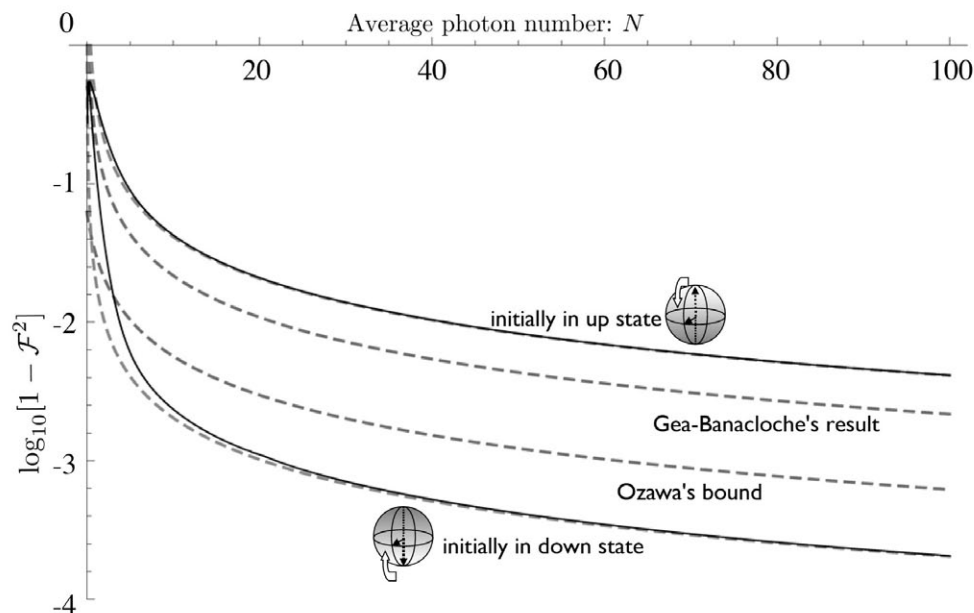


Fig. 1. Solid lines represent exact fidelity error rates for the initially up and initially down qubit states, respectively, plotted to the average photon number (N) of the field on a \log_{10} scale, along with the asymptotic curves for large N ($\sim 1/N$) and results of the former studies[1,2] as shown by dotted lines.

Monolithic Source of Polarization Entanglement Using Silicon Photonics

Nobuyuki Matsuda^{1,3}, Hanna Le Jeannic¹, Hiroshi Fukuda^{2,3}, Tai Tsuchizawa^{2,3},
Koji Yamada^{2,3}, and Hiroki Takesue¹

¹Optical Science Laboratory, ²NTT Microsystem Integration Laboratories,
³Nanophotonics Center

Integrated photonic waveguides, which provide a highly-stable and ultra-compact optical circuitry, is a promising candidate for a platform of scalable photonic quantum information processing (QIP) system [1]. Many QIP protocols are based on photonic quantum states encoded in polarization degree of freedom. Therefore, it is essential to implement integrated subsystems to generate, manipulate and measure polarization-encoded quantum states of light. This time we realized the first monolithic source of polarization entangled photon pairs by employing the silicon photonics technology [2].

The device consists of two silicon-wire waveguides (SWWs) connected by a silicon polarization rotator (SPR) [Fig. 1(a)]. In a SWW, a correlated pair of signal and idler photons is created following the annihilation of two pump photons via spontaneous four-wave mixing process. Here the pump, signal and idler photons are horizontally (H) polarized. The SPR has an off-axis double core structure of a Si inner core and a SiO_xN_y outer core. The SPR exhibits two orthogonal eigenmodes, which have different effective refractive indices and eigen-axes tilted at 45° with respect to the normal to the substrate [3]. The birefringence in the eigenmodes causes the polarization plane to rotate by an amount that depends on the length of the SPR. We obtain polarization-entangled photon pairs from the device by using optical pump pulses with +45° linear polarization as shown in Fig. 1. The polarization-mode dispersion and the polarization-dependent loss in a SWW, which potentially degrade the purity of polarization entanglement, can be automatically cancelled out in our device. We successfully obtained a maximally entangled state from the chip with a state fidelity as high as 94 %, which is well above the classical limit.

This work was supported by KAKENHI.

[1] A. Peruzzo et al., *Science* **329** (2010) 1500.

[2] N. Matsuda et al., *Sci. Rep.* **2** (2012) 817.

[3] H. Fukuda et al., *Opt. Express* **16** (2008) 2628.

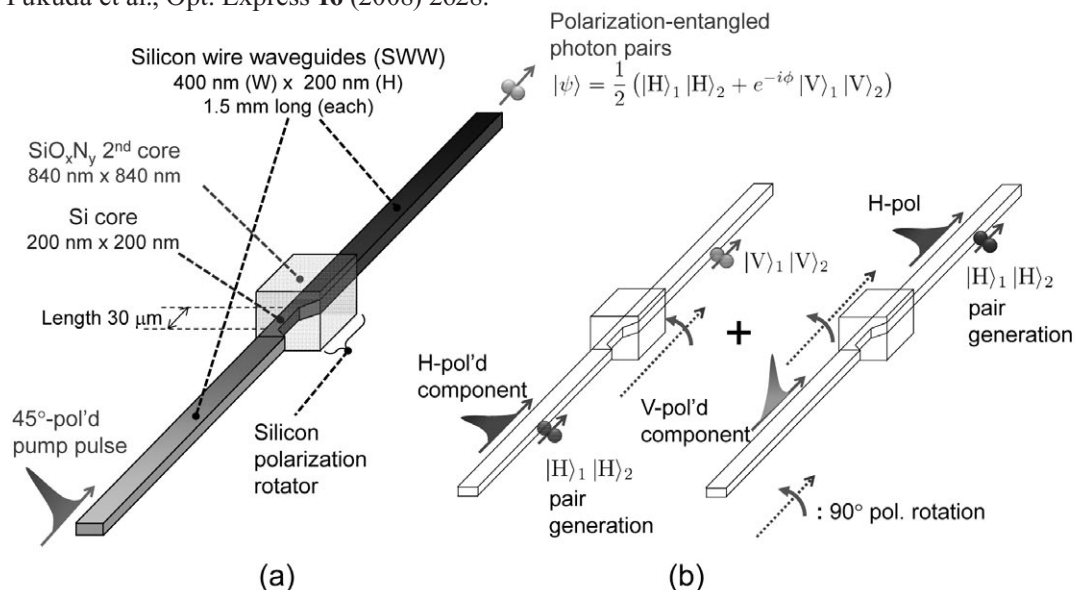


Fig. 1. (a) The monolithic polarization entanglement source and (b) its working principle. V represents the vertical polarization.

Bose-Einstein Condensate on a Persistent-Supercurrent Atom Chip

Hiromitsu Imai, Kensuke Inaba, Makoto Yamashita, and Tetsuya Mukai
Optical Science Laboratory

Ultra-cold atoms manipulated by electromagnetic field have been used widely for the applications of quantum information processing and quantum metrology. As a promising quantum device for full quantum control of an atomic state, a persistent-supercurrent atom chip allows us to trap atoms in extremely stable and tight potential. So far we have trapped atoms in a magnetic field of the persistent-supercurrent atom chip [1, 2]. In this year, we achieved ^{87}Rb Bose-Einstein condensate (BEC) by radio frequency induced evaporative cooling. This result paves the way for the development of quantum devices such as quantum memories and atom interferometers.

As shown in Fig. 1, Rb atoms were trapped in a potential generated by the magnetic field of a persistent supercurrent in a closed loop circuit and a bias magnetic field. To verify the condensation, we employed the time-of flight (TOF) imaging technique, and measured the momentum distribution of atoms released from the trapping potential after the evaporative cooling. Figure 2 (a) and (b) show the TOF image after 15 ms and the cross-section along the dotted line. These images were taken when a final radio frequency of the evaporative cooling ν_f was 1.770 MHz. The broad distribution indicates that the atomic gas remained in the thermal state. In Fig. 2 (c) and (d), a bimodal momentum distribution was observed as the onset of the BEC transition at $\nu_f = 1.750$ MHz. When ν_f was further decreased to 1.735 MHz [Figure 2 (e) and (f)], the thermal distribution was not observed and an almost pure condensate with a narrow distribution was obtained.

This work was supported by FIRST program, KAKENHI, and JST-CREST.

- [1] T. Mukai et al., Phys. Rev. Lett. **98** (2007) 260407.
[2] C. Hufnagel et al., Phys. Rev. A **79** (2009) 053641.

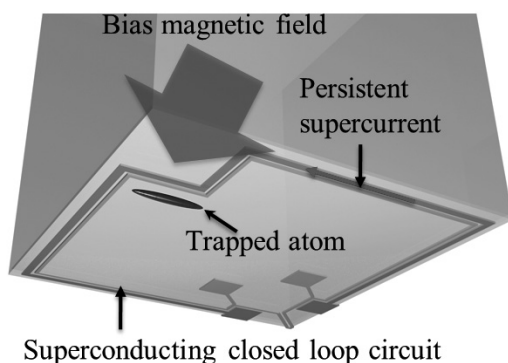


Fig. 1. Schematic diagram of atoms trapped on a persistent-supercurrent atom chip.

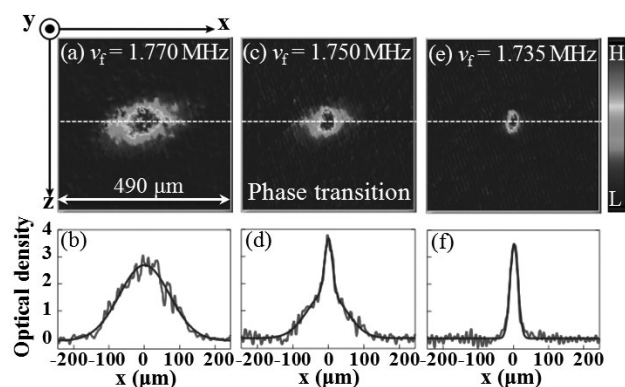


Fig. 2. TOF images after 15 ms (upper panels) and cross-sections of the optical density along the dotted lines (lower panels).

Ultrafast Surface Electron Dynamics on GaAs(001) Using Time-Resolved Photoelectron Spectroscopy Based on High-Order Harmonic Source

Katsuya Oguri, Keiko Kato, and Hiroki Mashiko
Optical Science Laboratory

High-harmonic generation (HHG) provides an attractive ultrashort light source of coherent radiation in the extreme-ultraviolet (EUV) and soft-x-ray regions of the spectrum, which is based on a highly nonlinear interaction between gaseous atoms and high peak power laser pulse with intensity of $10^{13} - 10^{15} \text{ W/cm}^2$ [1]. For the last two decades from the discovery of HHG, the HHG technology has made rapid progress resulting in a unique light source that possesses different characteristics from synchrotron radiation source and x-ray free electron laser. This opens the door to new widely applications of HHG source [2]. We have developed a technique of ultrafast surface photoelectron spectroscopy utilizing three characteristics of HHG including sharp spectral shape, ultrashort pulse duration, and wavelength of surface sensitivity. With this technique, we successfully measured a time-evolution of surface photovoltage effect on photo-excited GaAs(001) surface.

The photoelectron spectroscopy system uses a 100-fs titanium:sapphire laser system with a central wavelength of 790 nm operating at a 10 Hz repetition rate (Fig. 1). We selected the 59th harmonic pulse as the EUV probe by a pair of Mo/Si multilayer mirrors, and measured a photoelectron spectrum of GaAs(001) sample that was chemically etched. When the sample is excited with the laser pulse, we observed an energy shift of Ga 3d-core level photoelectron peak with about 200 meV towards higher binding energy, and its relaxation (Figs. 2(a) and (b)). This indicates that the surface potential changed due to the spatial separation of the electron-hole pair that was generated by the laser excitation, which is called as surface photovoltage (SPV) effect. Improving the temporal resolution of this scheme will enable us to investigate dynamics of SPV effect on semiconductor surface in femtosecond region [3].

[1] C. Winterfeldt et al., *Rev. Mod. Phys.* **80** (2008) 117.

[2] C. La-O-Vorakiat et al., *Phys. Rev. Lett.* **103** (2009) 257402.

[3] K. Oguri et al., *Jpn. J. Appl. Phys.* **51** (2012) 072401.

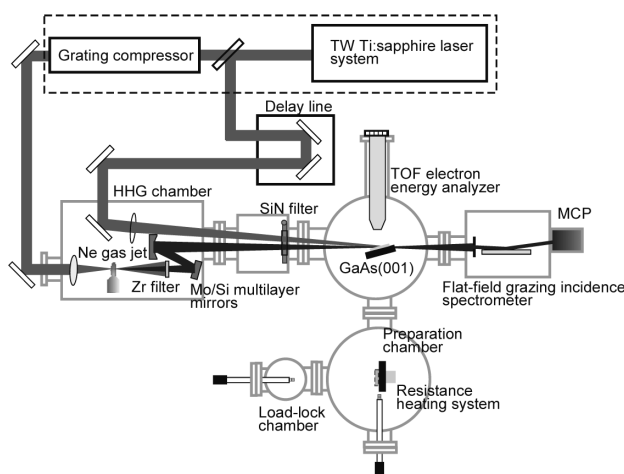


Fig. 1. Schematic illustration of the time-resolved surface photoelectron spectroscopy system.

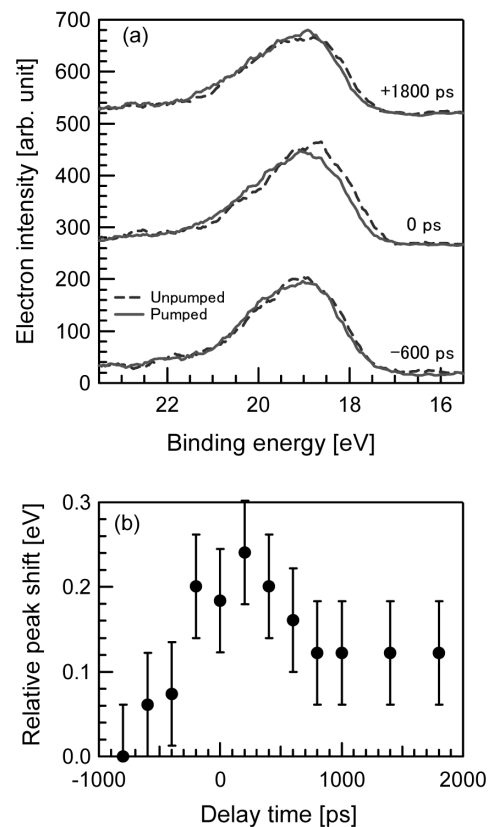


Fig. 2. Photo-induced transient change in the Ga-3d peak at various time delays (a), and its temporal evolution (b), respectively.

Coherent Manipulation of Moving Electron Spins Using Magnetic-Field-Free Electron Spin Resonance

Haruki Sanada, Yoji Kunihashi, and Koji Onomitsu*
Optical Science Laboratory, *Physical Science Laboratory

The most promising method of quantum information processing with electron spins is based on electron spin resonance (ESR), a technique commonly used both in research and for practical applications. However, the previously proposed spin manipulation methods require external magnetic fields, which are generated in spaces that greatly exceed the size of individual electrons, thus making these complex and inefficient techniques unsuitable for device applications. Here we demonstrate magnetic-field-free ESR achieved by using spin-orbit effective magnetic fields (\mathbf{B}^{SO}) [1].

The sample was an undoped 20-nm-thick GaAs/AlGaAs (001) quantum well (Fig. 1). A surface acoustic wave (SAW) beam generated by an interdigital transducer (IDT) produces an array of potential wires that move along y (\parallel [-110]) with a velocity of 2.97 km/s. A Ti film with 3- μm -wide slits deposited on the wafer partially screens the piezoelectric field and produces moving dots that travel along the channels formed beneath the slits. We performed Kerr microscopy to investigate spin transport along a straight and winding channels, the latter of which was designed to be close to the resonance condition. A circularly polarized pump light generates spin polarized electrons at certain position ($y = 0$) on the channels and linearly polarized light probes the Kerr rotation, which is proportional to the spin density at the probe position [2]. The sample was placed in an electro-magnet that generated a magnetic field (B_{ext}) along [110].

Figure 2 shows Kerr signals as a function of y and B_{ext} for the two channels. The oscillations observed for the straight channel are attributed to the spin precession induced by static magnetic fields. The effects induced by an oscillating spin-orbit field appear in the data for the winding channel; the precession phases show peculiar features at around $B_{\text{ext}} = 0$ and 46 mT. The Bloch simulations under \mathbf{B}^{SO} well reproduce the experimental results, and this proves the feasibility of the magnetic-field-free ESR. The technique will provide an efficient and flexible approach for the coherent control of flying spin information in solid-state devices.

This work was supported by KAKENHI.

[1] H. Sanada et al., Nature Physics **9** (2013) 280.

[2] H. Sanada et al., Phys. Rev. Lett. **106** (2011) 216602.

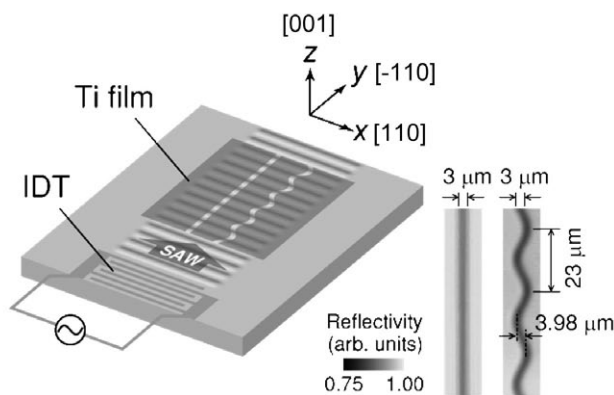


Fig. 1. Schematic view of the sample (left) and optical reflectivity images of the straight and winding channels (right).

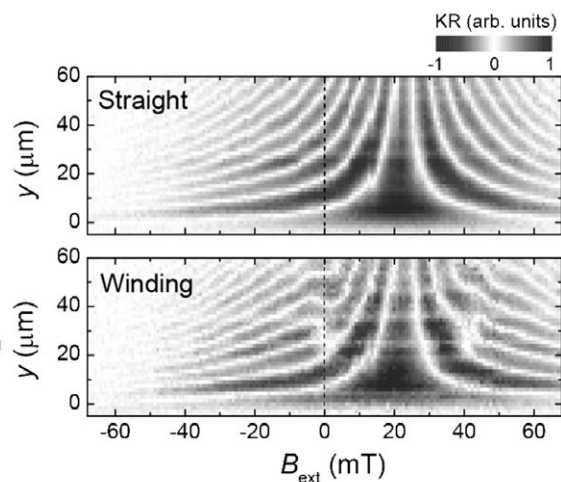


Fig. 2. Kerr rotation signals for the straight (upper) and winding (lower) channels plotted as a function of B_{ext} and y .

High-Efficiency Detection of Carrier-Envelope Offset Frequency with a Dual-Pitch PPLN Ridge Waveguide

Kenichi Hitachi, Atsushi Ishizawa, and Masaki Asobe
Optical Science Laboratory

A carrier-envelope offset (CEO) stabilized optical frequency comb provides dramatic progress in the field of precision spectroscopy and femtosecond pulse shaping. We have studied a 25-GHz-mode-spacing optical frequency comb provided by an externally phase-modulated laser diode, in which each frequency mode can be separated. This is an advantage compared to a common mode-locked laser whose repetition rate is smaller than a few hundred megahertz. For stabilizing a frequency comb, it is common to utilize a f -to- $2f$ self-referencing interferometer (SRI), in which one-octave bandwidth of the supercontinuum (SC) spectrum is required [1]. However, it is difficult to use this method for a phase-modulated frequency comb, because phase noise in the SC spectrum increases as the frequency departs from the original frequency. For this reason, we focus on a $2f$ -to- $3f$ SRI, in which $2/3$ -octave bandwidth of the SC spectrum is used. By utilizing a fiber laser for generating a SC spectrum and a dual-pitch (DP) periodically poled lithium niobate (PPLN) ridge waveguide for third-harmonic (TH) generation, we succeeded in detecting the CEO frequency with a high signal-to-noise ratio (SNR) (> 30 dB).

A DP-PPLN ridge waveguide device consists of two monolithically integrated segments with different quasi-phase matching (QPM) pitch sizes (Λ_1 , Λ_2) [Fig. 1(a)]. First, the second-harmonic (SH) light of the SC component at the frequency of f_1 is generated in the first segment with the pitch size of Λ_1 . Then, the sum frequency of the SH light ($2f_1$) and SC component of f_1' is generated in the second segment with Λ_2 [2]. Confinement of the SC light with a ridge waveguide structure and monolithically integrated design free from optical coupling loss enables TH generation with high efficiency.

In the experiment, a SC light (~ 300 mW) was generated by injecting the output from the fiber laser into a high nonlinear fiber, and spectrally separated with a dichroic mirror at the wavelength of 1500 nm. The SH (TH) light is generated from the short- (long-) wavelength component [~ 1200 (1800) nm] of the SC light. By detecting the heterodyne beat of the two outputs with a photodetector, we detected CEO signals with a SNR > 30 dB, which is high enough for stabilizing the CEO frequency [Fig. 1(b)]. In the future, we will detect and stabilize the CEO frequency of our developed externally phase-modulated laser with this technique.

[1] A. Ishizawa et al., *Opt. Express* **16** (2008) 4706.

[2] K. Hitachi et al., *Electron. Lett.* **49** (2013) 145.

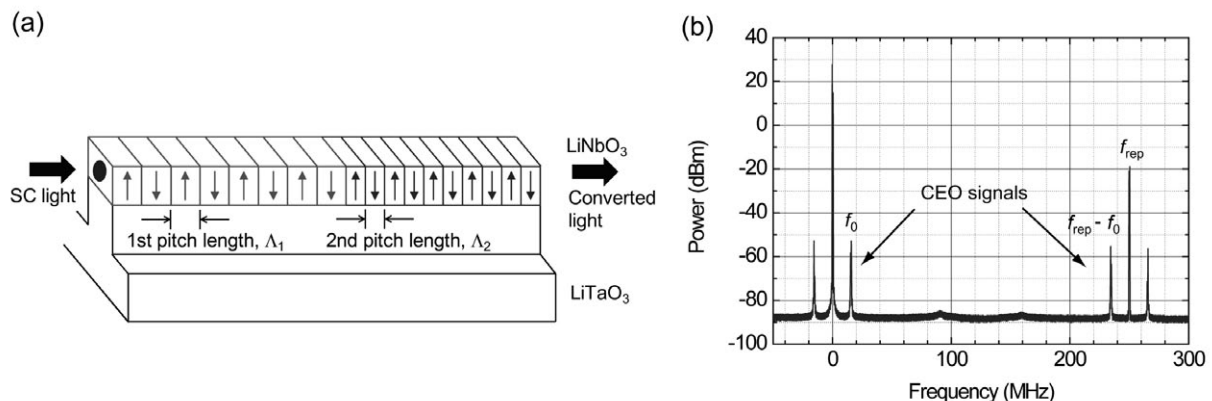


Fig. 1. (a) The schematic of a DP-PPLN ridge waveguide and (b) the detection of CEO signal.

Ultrafast Spontaneous Emission from Copper-Doped Silicon Nanocavity

Hisashi Sumikura^{1,2}, Eiichi Kuramochi^{1,2}, Hideaki Taniyama^{1,2}, and Masaya Notomi^{1,2}
¹Nanophotonics Center, ²Optical Science Laboratory

Impurities binding an exciton in Si show intense emission without phonon emission and attract a lot of attention as quantum bits (qubits) manipulated by light because of their long-lived spins. However, the light-impurity interaction is inefficient due to nonradiative processes including the Auger process. In this study, we focused on the combination of copper isoelectronic centers (Cu-IECs) and photonic crystal (PhC) nanocavities. The IEC originates from a bound exciton of deep impurities. Since the IEC is free from the Auger process, its emission quantum efficiency (QE) is high [1]. In addition, the high- Q nanocavity accelerates spontaneous emission from the Cu-IECs, which is known as the Purcell effect, and enhances the light-impurity interaction.

We have developed a novel method for doping the Cu-IECs to a SOI wafer. The Si PhC nanocavities were fabricated on the Cu-doped SOI wafer. Figure 1 shows photoluminescence (PL) spectra for the cavity with $Q = 7200$ and PL decays of the Cu-IECs. At 1227.5 nm, the emission peak of the Cu-IECs is found. The blue-side peak originates from the cavity resonance. When the cavity resonance approaches to the Cu-IEC line, the PL intensity and the decay rate of the Cu-IECs increase and take maximum values at zero detuning. Figure 2 shows PL decays and decay rates of the Cu-IECs in resonant cavities as a function of the Q/V value of the cavity. It is found that the decay rate is almost proportional to Q/V . This result proves the Purcell effect on the Cu-IECs because the theoretical estimation agrees well to the experimental data. In the highest- Q cavity ($Q = 16000$), the PL lifetime of the Cu-IECs is 1.1 ns, which is 30 times shorter than that in an unpatterned SOI sample. Since this PL lifetime is sufficiently smaller than the nonradiative lifetime around 40 ns, the QE may close to unity.

These results enable to develop novel fast and energy-efficient Si light emitting devices and quantum optical devices based on impurity qubits in Si.

[1] S. P. Watkins et al., Solid State Commun. **43** (1982) 687.

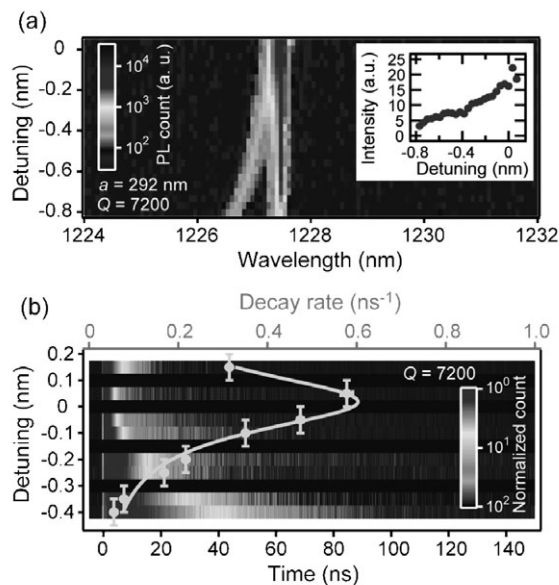


Fig. 1. (a) PL spectra for Cu-doped nanocavity. Inset shows the intensity of the Cu-IEC line. (b) PL decays and decay rates of the Cu-IECs.

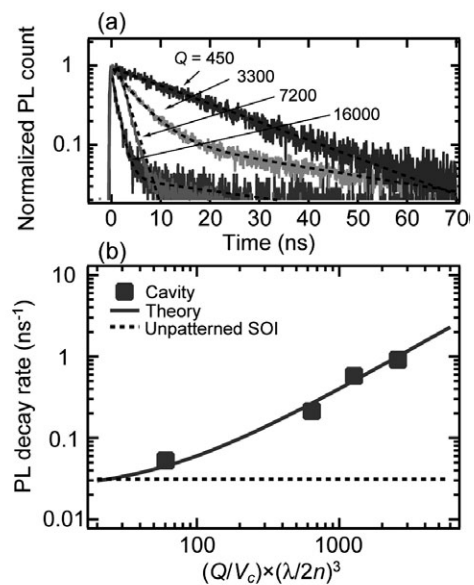


Fig. 2. (a) PL decays of the Cu-IECs in resonant cavities. (b) PL decay rates as a function of the Q/V values of the cavities. V is a mode volume.

Purcell-Enhanced Single Photon Emission at Telecom Wavelengths from Quantum-Dot Nanocavities

Muhammad Danang Birowosuto¹, Hisashi Sumikura^{1,2}, Shinji Matsuo^{2,3}, Hideaki Taniyama^{1,2}, and Masaya Notomi^{1,2}

¹Optical Science Laboratory, ²Nanophotonics Center, ³NTT Photonics Laboratories

A telecom-band (1.55 μm) single photon source is an important feature for the quantum communication networks, quantum repeaters, and all optical quantum information processing via optical fibers as this wavelength provides the lowest loss for long-distance transmission. Single InAs/InP quantum dot (QD) is an attractive emitter while a coupling of this single QD with a cavity yields a faster and brighter single photon source [1]. Single photon emission at 1.55 μm with shortest radiative recombination time of 1.12 ns from a single InAs QD in InP optical horn was previously reported [2]. However, there is no report for the single photon at 1.55 μm from the coupling between a single QD and a resonant cavity.

We demonstrate a fast single photon source at 1.55- μm telecom band from the coupling of the single QD with the cavity of the photonic crystals [3]. We combine the coupling of the biexciton (XX) of the single QD and the cavity, which may yield a faster single photon source than that of the exciton (X). Fig. 1 exhibits temperature-dependent photoluminescence spectra. The cavity is a line defect with hole-distance modulations. From the fit of the cavity peak, we obtain an experimental Q of 2,000. We observe that the QD biexciton and the cavity are in resonance at 22 K. At this temperature, we measure a very fast emission of 0.2 ns due to the Purcell effect with the five-fold emission rate enhancement, see Fig. 2. Photon intensity correlation measurement shows an antibunching with $g^{(2)}(0)$ of 0.1. Such fast single photon source at telecom band has a potential to improve the modulation rate of the long-distance quantum networks.

[1] A. J. Shields, Nature Photon. **1** (2007) 215.

[2] K. Takemoto et al., Appl. Phys. Express **3** (2010) 092802.

[3] M. D. Birowosuto et al., Sci. Rep. **2** (2012) 312.

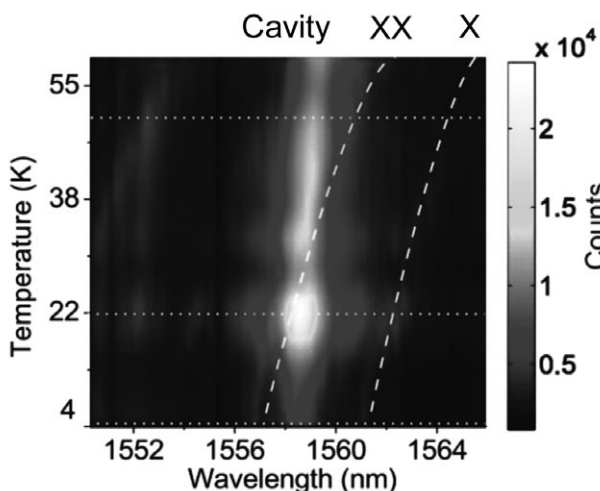


Fig. 1. Photoluminescence spectra at various temperatures for single QD in the cavity of PhC. X and XX denote the emission from exciton and biexciton, respectively.

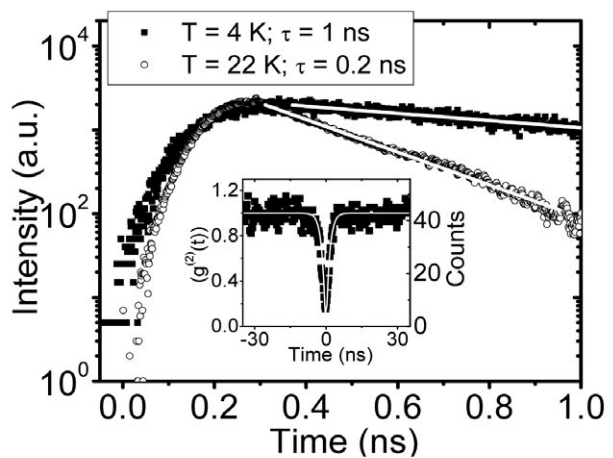


Fig. 2. Time resolved luminescence for single QD in the reference (squares) and the cavity (circles) of the PhC. The white lines are the exponential fits. The inset shows an antibunching at 22 K.

Lambda-Scale Embedded Active-Region Photonic-Crystal (LEAP) Lasers

Tomonari Sato^{1,2}, Koji Takeda^{1,2}, Akihiko Shinya^{1,3}, Kengo Nozaki^{1,3}, Hideaki Taniyama^{1,3}, Koichi Hasebe^{1,2}, Takaaki Kakitsuka^{1,2}, Masaya Notomi^{1,3}, and Shinji Matsuo^{1,2}
¹Nanophotonics Center, ²NTT Photonics Laboratories, ³Optical Science Laboratory

Photonic networks on CMOS chips have attracted a lot of attention as regards increasing transmission capacity, which is limited by the power consumption of electrical interconnects. The optical devices used for a photonic network on a CMOS chip are required to operate at an energy consumption of less than 10 fJ/bit. In this context, we have developed a photonic-crystal (PhC) nanocavity laser in which a small active region is embedded within an InP-based line defect waveguide. We call this a Lambda-scale Embedded Active-region PhC (LEAP) laser [1]. In this report, we report a LEAP laser with the lowest threshold current and energy consumption of any semiconductor laser operating at above room temperature, which we realized by reducing the leakage current.

Figure 1 shows a scanning electron microscope (SEM) image of a LEAP laser. An ultra-small active region, which consists of an InGaAlAs quantum-well structure, is embedded in a line defect in a 250 nm-thick InP PhC slab. The volume is $0.12 \mu\text{m}^3$. To reduce the leakage current through the sacrificial layer and the substrate, we change the sacrificial layer from InGaAs to InAlAs, because the bandgap of an InAlAs layer is larger than those of InP and InGaAs layers. We fabricate a lateral *p-i-n* junction by using Zn diffusion and Si ion implantation to inject carriers into the active region.

Figure 2 shows the light versus current characteristic and the spectrum under continuous-wave (CW) operation at 25°C. The threshold current and the maximum output power of the output waveguide were 7.8 μA and 9 μW , respectively. The lasing wavelength was 1567.8 nm at an injection current of 20 μA . We significantly reduced the threshold current by using InAlAs for the sacrificial layer because the threshold current of a LEAP laser with an InGaAs sacrificial layer was 390 μA . In addition, 12.5-Gbit/s direct modulation was achieved at an injection power of 174 μW and then the energy consumption was estimated to be 14 fJ/bit. Furthermore, we achieved high temperature operation up to 95°C with a LEAP laser [2].

This work was supported by NEDO.

[1] S. Matsuo et al., *Optics Express* **20** (2012) 3773.

[2] T. Sato et al., *IEEE Photonics Conference* (2012) WF-2.

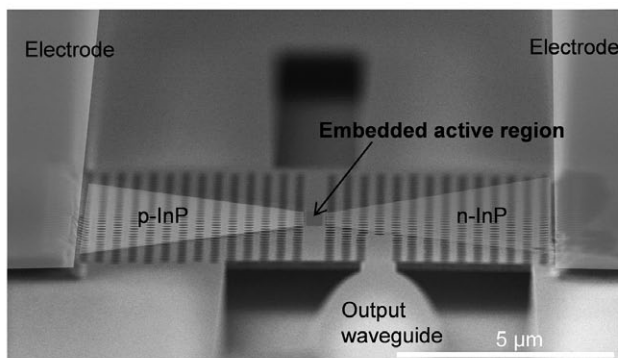


Fig. 1. SEM image of LEAP laser.

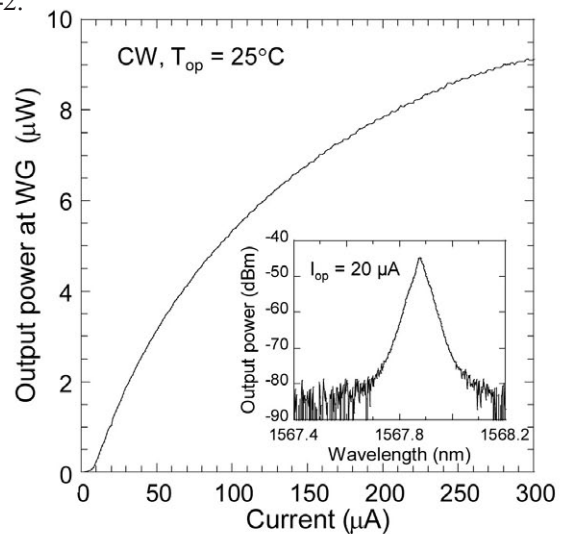


Fig. 2. Light-current characteristic of LEAP laser. Inset shows a spectrum at a current of 20 μA .

22-Gbit/s × 16-ch WDM Receiver Based on a Si-Ge-silica Monolithic Photonic Platform

Hidetaka Nishi^{1,2}, Rai Kou^{1,2}, Tatsuro Hiraki^{1,2}, Tai Tsuchizawa^{1,2}, Hiroshi Fukuda^{1,2},
Kotaro Takeda^{1,2}, Yasuhiko Ishikawa³, Kazumi Wada³, and Koji Yamada^{1,2}

¹Nanophotonics Center, ²NTT Microsystem Integration Laboratories, ³University of Tokyo

Towards the next generation of broad-band optical networks, systems based on wavelength-division multiplexing (WDM) are being discussed to offer flexible bandwidth allocation, which contributes to energy-efficient network operation. Silicon (Si) photonics WDM receivers are expected to provide small, cost-effective photonic-electronic integrated circuits with multiple channels and functionalities. Recently, we have developed an integrated WDM receiver on our unique Si-germanium (Ge)-silica monolithic platform [1], and demonstrated long-distance signal transmission with the fabricated device.

Figure 1 is a top-view of a fabricated WDM receiver. The arrayed-waveguide grating (AWG) wavelength filter comprises silicon-oxide (SiO_x) waveguides with a refractive index contrast of ~3 %. The waveguides are suitable for telecommunications applications because of their low loss and small temperature and polarization dependence. The AWG was connected to Si waveguides with the Ge photodetectors (PDs) using spot-size converters [2]. The Ge layer was grown by the UHV-CVD method [3]. SiO_x and SiO₂ layers for the AWG were deposited by the ECR plasma-enhanced CVD method, in which the process temperature lower than 200 degrees Celsius ensures that the AWG was constructed over the Ge layer without thermal damage. The footprint is about 1 cm². The insertion loss of the AWG is about 5.1 dB. The performance of Ge PD is as follows: dark current of 245 nA at -2 V, responsivity of about 1.2 A/W, and 3-dB down bandwidth of over 15 GHz, which is sufficient for over-20-Gbit/s data transmission. Figure 2 shows measured fiber-to-PD responsivity spectra, including fiber-coupling loss. The responsivity is 0.29 A/W and inter-channel crosstalk is -22 dB.

Next, we prepared 12.5-Gbit/s NRZ PRBS 2³¹-1 signal and input it into standard single-mode fibers with dispersion of 17 ps/km/nm at distances of 20, 40, and 60 km. After that, the signal was input into the AWG-PD device by butt coupling of a high-NA fiber. Figure 3 shows measured bit-error rate (BER) curves for various distances and a received eye pattern after 40-km transmission. We confirmed error-free signal transmission up to 40 km. The receiver sensitivity measured at the AWG input was -6.8 dBm for the BER of 10⁻⁹ after 40-km transmission. The experiment was performed at room temperature without thermal control. To the best of our knowledge, this is the first demonstration of long-distance signal transmission using Si photonic WDM receiver.

[1] H. Nishi et al., *Opt. Express* **20** (2012) 9312.

[2] T. Tsuchizawa et al., *J. Sel. Top. Quantum Electron.* **17** (2011) 516.

[3] S. Park et al., *IEICE Trans. Elect.* **E91-C** (2007) 181.

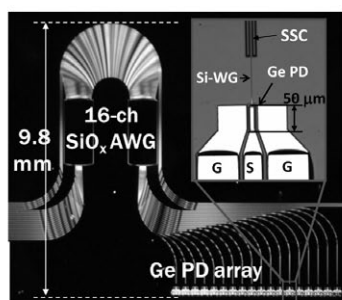


Fig. 1. Top view.

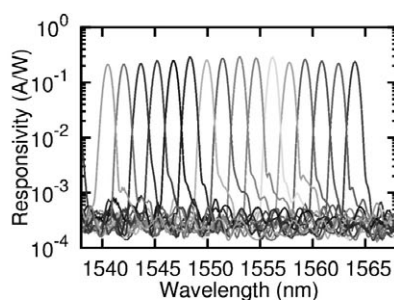


Fig. 2. Responsivity spectra.

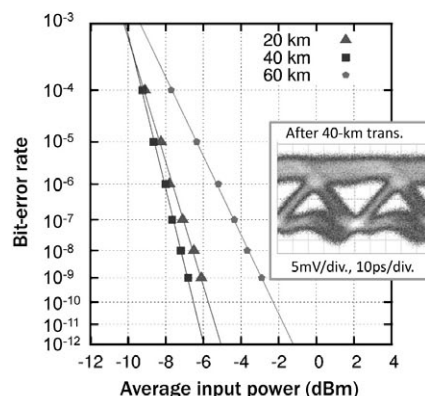


Fig. 3. BER curves.

II . Data

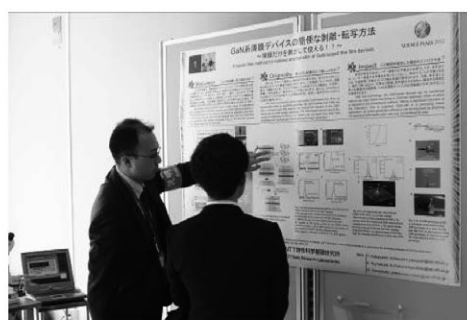
Science Plaza 2012

"Science Plaza 2012", an open-house event of NTT Basic Research Laboratories (BRL), was held at NTT Atsugi R&D Center on Friday, December 14th, 2012. Under the banner "Frontier Science: Open Door to the Future", Science Plaza aimed to disseminate our latest research accomplishments through various sections of people inside and outside of NTT and to gather diverse opinions.

Following an opening address from Dr. Toshiki Makimoto, the director of BRL, one of distinguished technical members of BRL, Dr. Shiro Saito gave a lecture on "Quantum Information Processing using Superconductivity — Development of Quantum Memory for Superconducting Quantum Bits". In the afternoon session, Prof. Koichi Kitazawa, Adviser to President, Japan Science and Technology Agency, gave a special lecture entitled "Renewable energies in the world". Each lecture was well-attended and followed by heated question-and-answer sessions.

As regards the poster exhibits, 52 posters, including 21 from NTT Microsystem Integration Laboratories, Photonics Laboratories, Communication Science Laboratories, and Energy and Environment Systems Laboratories presented our latest research accomplishments. While explaining the originality and impact as well as the future prospects of our research accomplishments, these posters were intensively discussed, and many meaningful opinions were heard. This year's "Lab Tour" — a guided tour of research facilities at NTT BRL that has been receiving high reputation from visitors over the years — took place at four different labs, so that as many people as possible could join the tour. This time we also opened a booth to show the NTT R&D recruitment system for job-seeking researchers and students. After all lectures, presentations, and exhibitions, a banquet was held in Center's dining room, where lively conversation among participants deepened their amity.

About 180 people from research institutes, universities, and general industries, as well as from NTT Group, attended Science Plaza 2012. Thanks to the efforts of all participants, the conference ended on a high note. We would thus like sincerely to express our gratitude to all of the participants.

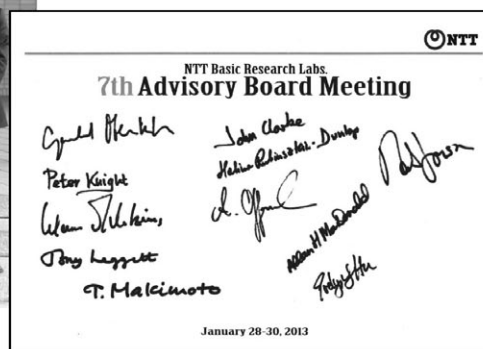


The 7th Advisory Board (Fiscal 2012)

The Advisory Board, an external committee whose role is to evaluate the work of NTT Basic Research Laboratories (BRL), met from January 28 - 30, 2013. This was the seventh meeting of the Advisory Board, which was first convened in 2001 to provide an objective evaluation of our research plans and activities to enable us to employ strategic management in a timely manner. On this occasion, we were happy to welcome six new members.

Over the course of the three days the board made valuable suggestions and comments in relation to our research and management activities. They commented that the research level is generally high on an international scale, and that it is important for us to maintain this top-level research and transmit information about our research achievements to the world. They also raised several issues related to human resources, the research budget and internal and external collaboration. We plan to make improvements based on these valuable suggestions.

At this meeting, the BRL researchers had a lunch with the board members and a poster session, where they had chances to present their researches to the board members. The poster session was performed with the dinner party where the board members and the BRL researchers were able to interact in a casual atmosphere. For the BRL and NTT executives, we organized a Japanese style dinner, which provided a good chance to discuss the future management strategy of NTT BRL from an international perspective. The next board meeting will be held in two years.



Board members	Affiliation	Research field
Prof. Abstreiter	Walter Schottky Inst.	Low-dim. physics
Prof. Clarke	Univ. California, Berkeley	Superconductor physics
Prof. Hu	Harvard Univ.	Nanodevice
Prof. Jonson	Göteborg Univ.	Condensed matter
Prof. Sir Knight	Imperial College	Quantum optics
Prof. Leggett	Univ. Illinois	Quantum physics
Prof. MacDonald	Univ. Texas	Condensed matter
Prof. Offenhäusser	Inst. Complex Systems	Nano-bio electronics
Prof. Rubinsztein-Dunlop	Univ. Queensland	Quantum electronics
Prof. von Klitzing	Max-Planck-Inst.	Semiconductor physics

Award Winners' List (Fiscal 2012)

The Commendation for Science and Technology by the Minister of Education, Culture, Sports, Science and Technology, The Young Scientists' Prize	N. Kumada	Many-body physics in two-dimensional systems formed in semiconductors	Apr. 17, 2012
JSAP Outstanding Presentation Award — 2012	N. Matsuda	On-chip polarization-entangled photon pair source	May 11, 2012
International conference on topological quantum phenomena 2012 Poster award and poster preview award	H. Irie	Josephson characteristics of superconducting quantum point contact	May 20, 2012
Fifth International Conference on Optical, Optoelectronic and Photonic Materials and Applications Poster Paper Award	H. Kudo (*) Y. Ogawa (*) T. Tanabe (*) A. Yokoo (*) Keio University	Fabrication of whispering gallery mode cavities using crystal growth	June 3, 2012
JSAP Young Scientist Award	S. Tanabe	Half-Integer Quantum Hall Effect in Gate-Controlled Epitaxial Graphene Devices	Sep. 11, 2012
Photonics in Switching 2012 Award for SC1 best paper	K. Nozaki A. Shinya M. Notomi S. Matsuo T. Sato Y. Suzuki T. Segawa R. Takahashi	First demonstration of 4-bit, 40-Gb/s optical RAM chip using integrated photonic crystal nanocavities	Sep. 13, 2012
The 141st Committee on Microbeam Analysis of Japan Society for the Promotion of Science Sakaki Award	H. Hibino	Characterization and growth control of low-dimensional materials using low-energy electron microscopy	Sep. 27, 2012

International Workshop on Nitride Semiconductors 2012 Best Paper Award	Y. Taniyasu J.-F. Carlin* A. Castiglia* R. Butté* N. Grandjean*	AlInN/GaN MQW UV-LEDs	Oct. 19, 2012
	(*) Ecole Polytechnique Fédéral de Lausanne		
Fellowship of the American Physical Society	W. J. Munro	For extensive contributions to applied quantum information	Nov. 3, 2012
26th Diamond Symposium Oral Session Best Award	K. Hiramata H. Sato Y. Harada H. Yamamoto M. Kasu	NO ₂ -adsorbed H-terminated diamond FETs thermally stabilized by Al ₂ O ₃ passivation	Nov. 20, 2012
IEEE Fellow	M. Notomi	For leadership in the development of photonic crystals and applications	Jan. 1, 2013
Hot Article Award, Analytical Sciences	Y. Ueno K. Furukawa K. Hayashi M. Takamura H. Hibino E. Tamechika	Graphene-modified Interdigitated Array Electrode: Fabrication, Characterization, and Electrochemical Immunoassay Application	Jan. 10, 2013
33th JSAP Outstanding Presentation Award — 2013	H. Sumikura	Purcell effect on copper isoelectronic centers in silicon photonic crystal cavities	Mar. 27, 2013
Superconductivity Division of Japan Society of Applied Physics Young Scientist Award for an Excellent Article	Y. Krockenberger	Molecular Beam Epitaxy and Transport Properties of Infinite-Layer Sr _{0.90} La _{0.10} CuO ₂ Thin Films	Mar. 28, 2013

In-house Award Winners' List (Fiscal 2012)

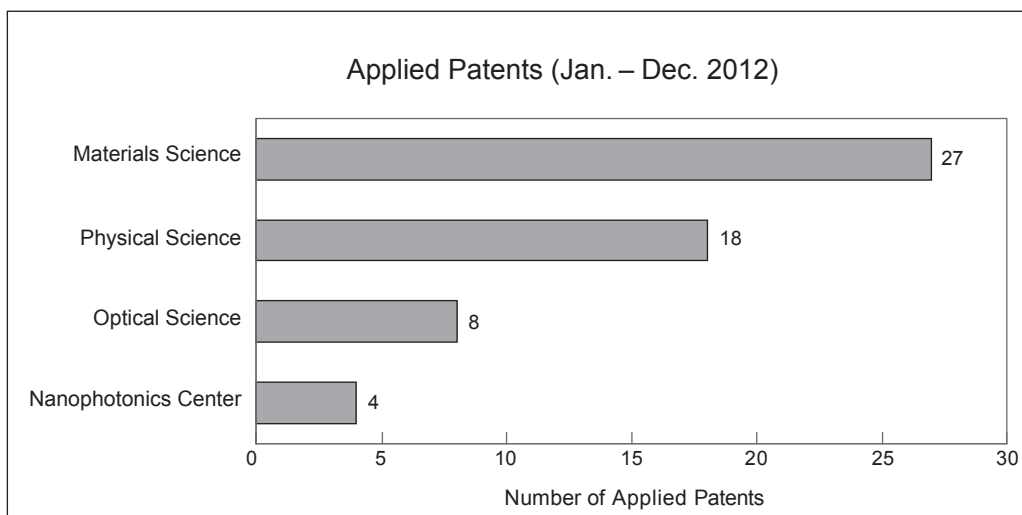
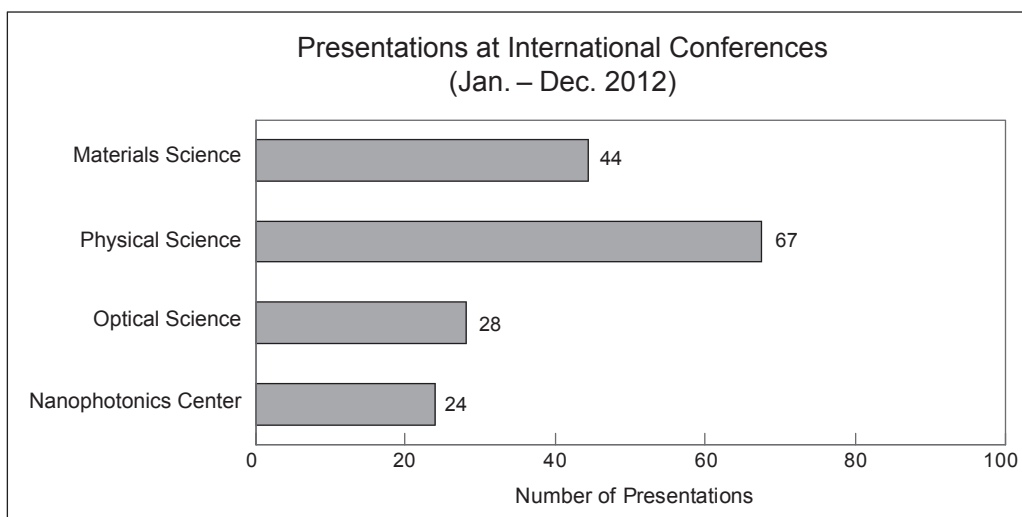
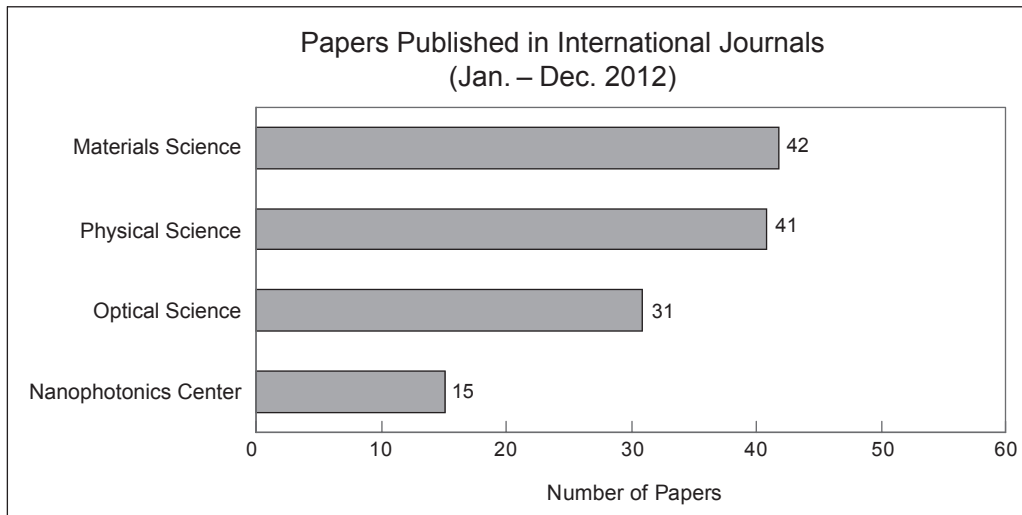
NTT Science and Core Technology Laboratory Group Director Award	Y. Kobayashi K. Kumakura T. Akasaka Y. Krockenberger H. Yamamoto	Development of a process for release and transfer of GaN-based devices	Dec. 19, 2012
NTT Science and Core Technology Laboratory Group Director Award	T. Sato K. Takeda A. Shinya K. Nozaki S. Matsuo	Current-injection photonic-crystal laser for high density optical interconnection	Dec. 19, 2012
NTT Science and Core Technology Laboratory Group Director Award	S. Tsukada H. Nakashima A. Shimada K. Sumitomo	Invention of the conductive polymer combined thread for the biomedical electrodes	Dec. 19, 2012
BRL Director Award Award for Achievements	Y. Kobayashi K. Kumakura T. Akasaka	Development of a process for release and transfer of GaN-based devices using layered BN	Mar. 25, 2013
BRL Director Award Award for Achievements	S. Tsukada H. Nakashima A. Shimada K. Torimitsu K. Sumitomo	Development of the conductive polymer combined Silk fiber for the biomedical electrodes	Mar. 25, 2013
BRL Director Award Award for Achievements	I. Mahboob H. Okamoto D. Hatanaka K. Nishiguchi K. Onomitsu A. Fujiwara H. Yamaguchi	Proposition and realization of novel devices based on compound semiconductor electromechanical resonators	Mar. 25, 2013
BRL Director Award Award for Encouragement	S. Tanabe	Contribution to clarifying electronic transport properties of epitaxial graphene on SiC	Mar. 25, 2013
BRL Director Award Award for Excellent Papers	K. Nozaki A. Shinya S. Matsuo Y. Suzuki T. Segawa T. Sato Y. Kawaguchi R. Takahashi M. Notomi	"Ultralow-power all-optical RAM based on nanocavities" Nature Photonics 6, 248-252 (2012).	Mar. 25, 2013

BRL Director Award Award for Excellent Papers	N. Matsuda H. Le Jeannic H. Fukuda T. Tsuchizawa W. J. Munro K. Shimizu K. Yamada Y. Tokura H. Takesue	"A monolithically integrated polarization entangled photon pair source on a silicon chip" Scientific Reports 2, 817 (2012)	Mar. 25, 2013
--	--	---	------------------

BRL Director Award Award for Excellent Papers	K. Azuma G. Kato	"Optimal entanglement manipulation via coherent-state transmission" Physical Review A 85, 060303(R) (2012)	Mar. 25, 2013
--	---------------------	---	------------------

Numbers of Papers, Presentations and Patents (2012)

The numbers of papers published in international journals, presentations at international conferences and applied patents in year 2012 amounted to 129, 163, and 57, respectively. The numbers for each research area are as follows;



The numbers of research papers published in the major journals are shown below.

Journals	(IF2011*)	Numbers
Japanese Journal of Applied Physics	1.058	15
Applied Physics Letters	3.844	11
Physical Review B	3.691	11
Applied Physics Express	3.013	10
Physical Review A	2.878	7
Journal of Applied Physics	2.168	6
Optics Express	3.587	5
Nano Letters	13.198	3
Nature Photonics	29.278	2
Physical Review Letters	7.37	2
The Journal of Physical Chemistry Letters	6.213	2
Langmuir	4.186	2
New Journal of Physics	4.177	2
Nature	36.28	1
Science	31.201	1
Nature Nanotechnology	27.27	1
Nature Physics	18.967	1
Advanced Materials	13.877	1
ACS Nano	11.421	1
Nature Communications	7.396	1
Biosensors and Bioelectronics	5.602	1
Carbon	5.378	1
PLoS One	4.092	1

*IF2011: Impact Factor 2011 (Thomson Reuters Journal Citation Reports® 2011)

The average IF2011 for all research papers from NTT Basic Research Laboratories is 4.74.

The numbers of presentations in the major conferences are shown below.

Conferences	Numbers
31st International Conference on the Physics of Semiconductors	20
2012 International Conference on Solid State Devices and Materials	10
The 17th International Conference on Molecular Beam Epitaxy	7
International Workshop on Nitride Semiconductors 2012	6
11th International Conference on Quantum Communication, Measurement and Computing	4
2012 Materials Research Society Spring Meeting and Exhibit	4
The 20th International Conference on High Magnetic Fields in Semiconductor Physics	4
25th International Microprocesses and Nanotechnology Conference	3
2012 Workshop on Innovative Nanoscale Devices and Systems	3
The American Physical Society March Meeting 2012	3
New Diamond and Nano Carbons Conference 2012	3
The 7th International Conference on Physics and Applications of Spin-related Phenomena in Semiconductors	3

List of Invited Talks at International Conferences (2012)

I. Materials Science Laboratory

- (1) Y. Kashimura, K. Furukawa, and K. Torimitsu, "Control of molecule transport utilizing lipid bilayer self-spreading on micro/nano-patterned surface", The 6th International Symposium on Medical, Bio- and Nano-Electronics, Sendai, Japan (Mar. 2012).
- (2) K. Hirama, M. Kasu, and Y. Taniyasu, "Nitride/diamond heterostructure: growth and device application", New Diamond and Nano Carbons Conference (NDNC 2012), San Juan, Puerto Rico (May 2012).
- (3) N. Kasai, A. Shimada, S. Tsukada, A. Tanaka, Y. Kashimura, K. Sumitomo, and K. Torimitsu, "Micro/nano-fabrication for biological interface", The 7th International Symposium on Organic Molecular Electronics (ISOME2012), Musashino, Japan (June 2012).
- (4) A. D. Malay, J. G. Heddle, S. Tomita, K. Iwasaki, N. Miyazaki, K. Sumitomo, H. Yanagi, I. Yamashita, and Y. Uraoka, "A gold nanoparticle-catalysed artificial protein capsid", The 6th International Conference on Gold Science Technology and its Applications (GOLD2012), Tokyo, Japan (Sep. 2012).
- (5) Y. Kobayashi, K. Kumakura, T. Akasaka, H. Yamamoto, and T. Makimoto, "Layered boron nitride as a release layer for mechanical transfer of GaN-based devices", Crystal & Graphene Science Symposium, Boston, U.S.A. (Sep. 2012).
- (6) H. Hibino, S. Tanabe, and H. Kageshima, "Carrier transport in epitaxial and quasi-freestanding graphene on SiC", International Union of Materials Research Societies-International Conference on Electronic Materials (IUMRS-ICEM2012), Yokohama, Japan (Sep. 2012).
- (7) T. Akasaka, H. Goto, Y. Kobayashi, and H. Yamamoto, "Extremely narrow photoluminescence line from ultrathin InN single quantum well on step-free GaN surface", International Workshop on Nitride semiconductors, Sapporo, Japan (Oct. 2012).
- (8) Y. Kobayashi, K. Kumakura, T. Akasaka, H. Yamamoto, and T. Makimoto, "Layered boron nitride as a release layer for mechanical transfer of GaN-based devices", International Workshop on Nitride semiconductors, Sapporo, Japan (Oct. 2012).
- (9) T. Akasaka, Y. Kobayashi, C. H. Lin, and H. Yamamoto, "Study of nucleus and spiral growth mechanisms of GaN using selective-area MOVPE on GaN bulk substrate", Intensive Discussion on Growth of Nitride Semiconductors, Sendai, Japan (Oct. 2012).
- (10) Y. Ueno, K. Furukawa, K. Matsuo, K. Hayashi, S. Inoue, H. Hibino, and E. Tamechika, "Aptamer Modified Graphene Oxide Installed in a Microchannel Device: A New Lab-on-a-chip Protein Detection System", 6th International Symposium on Nanomedicine (ISNM2012), Matsue, Japan (Nov. 2012).
- (11) K. Furukawa and H. Hibino, "AFM Study of Collision of Self-spreading Lipid Bilayers within Micro Pattern", 20th International Colloquium on Scanning Probe Microscopy, Naha, Japan (Dec. 2012).

II. Physical Science Laboratory

- (1) S. Saito, X. Zhu, Y. Matsuzaki, W. J. Munro, M. S. Everitt, T. Shimooka, N. Mizuochi, K. Nemoto, and K. Semba, "Coherent coupling between a superconducting flux qubit and a spin ensemble", Pathbreaking Phase Sciences in Superconductivity 2012 (PPSS2012), Osaka, Japan (Jan. 2012).
- (2) K. Nishiguchi, "Nanoscale electronic devices with low power consumption and high functionality", The Japan-France Frontiers of Engineering Symposium 2012 (JFFoE2012), Kyoto, Japan (Feb. 2012).
- (3) X. Zhu, S. Saito, A. Kemp, K. Kakuyanagi, S. Karimoto, H. Nakano, W. J. Munro, Y. Tokura, M. S. Everitt, K. Nemoto, M. Kasu, N. Mizuochi, and K. Semba, "Coherent coupling of a superconducting flux qubit to an electron spin ensemble in diamond", Quantum Information and Measurement (QIM2012), Berlin, Germany (Mar. 2012).
- (4) L. Tiemann, G. Gamez, N. Kumada, and K. Muraki, "NMR Investigation of the $\nu = 5/2$ Fractional Quantum Hall State", International conference on topological quantum phenomena 2012 (TQP2012), Nagoya, Japan (May 2012).
- (5) H. Yamaguchi, I. Mahboob, and H. Okamoto, "Piezoelectric parametric resonators", NEMS-Barcelona, Barcelona, Spain (May 2012).
- (6) A. Fujiwara, G. Yamahata, K. Nishiguchi, G. P. Lansbergen, and Y. Ono, "Silicon Single-Electron Transfer Devices: Ultimate Control of Electric Charge", Silicon Nanoelectronics Workshop (SNW2012), Hawaii, U.S.A. (July 2012).
- (7) L. Tiemann, G. Gamez, N. Kumada, and K. Muraki, "Nuclear magnetic resonance studies of the electron spin polarisation in the $N = 0$ and $N = 1$ Landau levels", The 20th International Conference on High Magnetic Fields in Semiconductor Physics (HMF20), Chamonix Mont-Blanc, France (July 2012).
- (8) H. Yamaguchi, I. Mahboob, and H. Okamoto, "Parametric mode-coupling and its application to signal processing in GaAs/AlGaAs electromechanical resonators", 31st International Conference on the Physics of Semiconductors (ICPS2012), Zurich, Switzerland (July 2012).
- (9) S. Saito, X. Zhu, Y. Matsuzaki, W. J. Munro, K. Kakuyanagi, T. Shimooka, N. Mizuochi, K. Nemoto, and K. Semba, "Coherent operations in a superconductor-diamond hybrid system", 19th Central European Workshop on Quantum Optics (CEWQO2012), Sinaia, Romania (July 2012).
- (10) H. Yamaguchi, I. Mahboob, H. Okamoto, and K. Onomitsu, "Semiconductor Heterostructures for Novel Electromechanical Devices", Materials Science Week 2012 (MSW2012), Sendai, Japan (Nov. 2012).

III. Optical Science Laboratory

- (1) Y. Tokura, "Coherent control and detection of spin qubits in semiconductor with magnetic field engineering", APS March Meeting, Boston, U.S.A. (Feb. 2012).
- (2) W. J. Munro and K. Nemoto, "Inferring superposition and entanglement in evolving systems", The 2nd Institute of Mathematical Statistics Asia Pacific Rim Meeting, Tsukuba, Japan (July 2012).
- (3) M. Yamashita and K. Inaba, "Diverse quantum phases of Bose-Fermi mixtures trapped in an optical lattice", The 21st International Laser Physics Workshop (LPHYS'12), Calgary, Canada (July 2012).
- (4) K. Oguri, H. Nakano, Y. Okano, T. Nishikawa, K. Kato, A. Ishizawa, T. Tsunoi, H. Gotoh, K. Tateno, and T. Sogawa, "Ultrafast diagnostics of photo-excited processes in solid using femtosecond laser-based soft X-ray pulse sources", 8th International Conference on Photo-Excited Processes and Applications (ICPEPA-8), Rochester NY, U.S.A. (Aug. 2012).
- (5) W. J. Munro and K. Nemoto, "Weak force detection using superposed coherent states", International Workshop on Entangled Coherent State and Its Application to Quantum Information Science - Towards Macroscopic Quantum Communication, Tamagawa University, Tokyo, Japan (Nov. 2012).
- (6) K. Azuma, "Entanglement shared via coherent-state transmission", Quantum Science Symposium 2012, Cambridge, U.K. (Nov. 2012).
- (7) T. Mukai, "Superconducting Atom Chip in NTT", The 2nd Atom Chip Workshop in Pangkil, Indonesia (Dec. 2012).
- (8) H. Shibata, "Fabrication of Superconducting Strip Photon Detector using MgB₂", International Workshop on Superconducting Sensors and Detectors (IWSSD2012), Daejeon, Korea (Dec. 2012).
- (9) W. J. Munro, S. Saito, X. Zhu, R. Amsuss, Y. Matsuzaki, K. Kakuyanagi, T. Shimooka, N. Mizuochi, K. Nemoto, and K. Semba, "Realizing Quantum Memories for Superconducting Qubits: Storage and Retrieval of Entangled Quantum States", EQUUS Annual Workshop, Wollongong, Australia (Dec. 2012).

IV. Nanophotonics Center

- (1) M. Notomi, K. Nozaki, S. Matsuo, A. Shinya, T. Sato, and H. Taniyama, "fJ/bit integrated nanophotonics towards dense photonic network on chip", SPIE Photonics West 2012, San Francisco, U.S.A. (Jan. 2012).
- (2) S. Matsuo, "High-speed directly modulated buried heterostructure photonic crystal lasers", Photonic West 2012, San Francisco, U.S.A. (Jan. 2012).
- (3) M. Notomi, K. Nozaki, S. Matsuo, A. Shinya, T. Sato, and H. Taniyama, "fJ/bit integrated nanophotonics for photonic network on chip", The Fourth International Conference on Metamaterials, Photonic Crystals, and Plasmonics (META'12), Paris, France (Apr. 2012).
- (4) M. Notomi, K. Nozaki, S. Matsuo, A. Shinya, E. Kuramochi, T. Sato, H. Taniyama, and C-H. Chen, "Nonlinear Optical Functions of Photonic Crystals for Ultralow-power Photonic Processing", CLEO: 2012, San Jose, U.S.A. (May 2012).
- (5) M. Notomi, K. Nozaki, S. Matsuo, A. Shinya, J. Kim, K. Takeda, E. Kuramochi, T. Sato, and H. Taniyama, "Nanophotonic Devices Based on Photonic Crystal", International Conference on Photonic and Electromagnetic Structures (PECS-X), Santa Fe, U.S.A. (June 2012).
- (6) A. Yokoo, T. Tanabe, E Kuramochi, and M. Notomi, "Fabrication of photonic crystal cavity by using a nanoprobe", The 7th International Symposium on Organic Molecular Electronics, Tokyo, Japan (June 2012).
- (7) K. Nozaki, A. Shinya, S. Matsuo, T. Sato, Y. Suzuki, T. Segawa, R. Takahashi, and M. Notomi, "Integrable ultralow-power nanophotonic devices on InP photonic crystals", OSA Integrated Photonics Research, Silicon and Nano-Photonics (IPR2012), Colorado Springs, U.S.A. (June 2012).
- (8) T. Tsuchizawa, H. Nishi, R. Kou, H. Fukuda, H. Shinjima, Y. Ishikawa, K. Wada, and K Yamada, "Silicon-silica Monolithic Photonic Integration for Telecommunications Applications", Integrated Photonics Research, Silicon and Nano Photonics (IPR2012), Colorado, U.S.A. (June 2012).
- (9) M. Notomi, K. Nozaki, S. Matsuo, A. Shinya, E. Kuramochi, T. Sato, J. Kim, K. Takeda, and H. Taniyama, "Ultralow-power integrated nanophotonics for future chips", The 17th Opto Electronics and Communications Conference (OECC2012), Busan, Korea (July 2012).
- (10) K. Yamada, T. Tsuchizawa, H. Nishi, R. Kou, H. Shinjima, H. Fukuda, T. Hiraki, Y. Ishikawa, and K. Wada, "Silicon Photonics for Telecommunications", The 17th Opto Electronics and Communications Conference (OECC2012), Busan, Korea (July 2012).
- (11) M. Notomi, K. Nozaki, S. Matsuo, A. Shinya, E. Kuramochi, T. Sato, K. Takeda, J. Kim, H. Taniyama, "Ultralow-power nanophotonic devices based on buried-heterostructure photonic-crystal nanocavities", 24th International Conference on Indium Phosphide and Related Materials (IPRM2012), Santa Barbara, U.S.A. (Aug. 2012).
- (12) M. Notomi, K. Nozaki, S. Matsuo, A. Shinya, E. Kuramochi, T. Sato, A. Yokoo, J. Kim, K. Takeda, and H. Taniyama, "fJ/bit Integrated Nanophotonics based on Photonic Crystals", International Conference on Electronic Materials-International Union of Material Research Societies (IUMRS-ICEM2012), Yokohama, Japan (Sep. 2012).
- (13) K. Nozaki, A. Shinya, S. Matsuo, T. Sato, K. Takeda, C-H. Chen, Y. Suzuki, T. Segawa, R. Takahashi, and M. Notomi, "Integrable All-Optical Random-Access Memories on InP-based Photonic Crystal Platform", IEEE Photonics Conference (IPC2012), Burlingame, U.S.A. (Sep. 2012).

- (14) K. Yamada, T. Tsuchizawa, H. Nishi, R. Kou, T. Hiraki, H. Fukuda, Y. Ishikawa, and K. Wada, "Silicon/Ge/Silica Monolithic Photonic Integration for Telecommunications Applications", 2012 International Conference on Solid State Devices and Materials (SSDM2012), Kyoto, Japan (Sep. 2012).
- (15) S. Matsuo, "Ultra-low operating energy lasers and switches for optical interconnection", Photonic in Switching 2012, Ajaccio-Corsica, France (Sep. 2012).
- (16) S. Matsuo, K. Takeda, T. Sato, M. Notomi, A. Shinya, K. Nozaki, H. Taniyama, K. Hasebe, and T. Kakitsuka, "Electrically-pumped Photonic Crystal Lasers for Optical Communications", The 38th European Conference on Optical Communications (ECOC2012), Amsterdam, The Netherlands (Sep. 2012).
- (17) S. Matsuo, "Electrically driven photonic crystal nanocavity laser", IEEE 23rd International Semiconductor Laser Conference (ISLC2012), San Diego, U.S.A. (Oct. 2012).
- (18) K. Yamada, T. Tsuchizawa, H. Nishi, R. Kou, H. Fukuda, T. Hiraki, Y. Ishikawa, and K. Wada, "Si/Ge/Silica Monolithic Photonic Integration Platform for Telecommunications Applications", Asia Communications and Photonics Conference 2012 (ACP2012), Guangzhou, China (Nov. 2012).
- (19) S. Matsuo, "Electrically Driven Photonic Crystal Lasers for On-Chip Interconnect", The 2nd International Symposium on Photonics and Electronics Convergence (ISPEC2012), Tokyo, Japan (Dec. 2012).

**Research Activities in NTT-BRL
Editorial Committee**

NTT Basic Research Laboratories

3-1Morinosato Wakamiya, Atsugi

Kanagawa, 243-0198 Japan

URL: <http://www.brl.ntt.co.jp/>